Research Article

Mid-Pleistocene drainage rearrangement of the Dadu River in response to plate convergence in southeastern Tibet

Yong Zheng[a,b,c,d] , Haibing Li[a,b,c]* , Jiawei Pan[a,b,c], Zheng Gong[e], Ping Wang[f], Ya Lai[a,b,c], Zhongbao Zhao[a,b,c] and Fucai Liu[a,b,c]

[a]Key Laboratory of Deep-Earth Dynamics, Ministry of Natural Resources, Institute of Geology, Chinese Academy of Geological Sciences, Beijing, China, 100037; [b]Southern Marine Science and Engineering Guangdong Laboratory, Guangzhou, China, 511458; [c]Jiangsu Donghai Continental Deep Hole Crustal Activity National Observation and Research Station, Jiangsu, China, 222300; [d]Department of Geography, Korea University, Seoul, Korea, 02841; [e]Institute of Geophysics, China Earthquake Administration, Beijing, China, 100081 and [f]Geophysical Exploration Center, China Earthquake Administration, Zhengzhou, China, 450002

Abstract

The rearrangement of drainage basins provides critical insight into crustal deformation and geodynamic mechanisms. Near the southeastern boundary of the Tibetan Plateau, the Dadu River abruptly shifts from south- to east-flowing, providing important implications for regional tectonogeomorphic development since the mid-Pleistocene. South of the bend, the headwaters of the Anning River occupy an unusually wide valley. Field investigations show that large quantities of fluvial/lacustrine sediments are widespread along the Dadu and Anning rivers and are exposed at their drainage divide. Detrital zircon U-Pb age patterns confirm that these fluvial/lacustrine sediments are the remnants of the paleo-Dadu River, which strongly suggests that the paleo-Dadu River originally flowed southward into the Anning River. The cosmogenic nuclide burial ages of the lacustrine sediments along the Dadu and Anning rivers suggest deposition of these sediments from separate dammed lakes ca. 1.2 Ma ago, ca. 0.6 Ma ago, and ca. 0.9 Ma ago from north to south, respectively. Provenance and burial-age studies indicate that reorganization of the Dadu drainage occurred within the last 0.6 Ma. We propose that this drainage reorganization in southeastern Tibet resulted from progressive convergence between the India and Eurasian plates during the Pleistocene.

Keywords: Dadu River, Tectonogeomorphic development, Fluvial/lacustrine sediments, Detrital zircon U-Pb age, Cosmogenic nuclide, Drainage reorganization

INTRODUCTION

Progressive convergence between the India and Eurasia plates since early Cenozoic has resulted in ∼2000–3000 km shortening of crustal material (Molnar et al., 1993). Crustal thickening beneath the Tibetan Plateau has absorbed the material to a large extent. Part of the material was accommodated by lateral movement (Fig. 1A), such as along the Ailao Shan-Red River shear zone 35–17 Ma ago (Leloup et al., 1995). The dynamic flow model proposes an additional way to accommodate the material: either the high-temperature lower crustal material (Clark and Royden, 2000) or asthenospheric flow (Shi et al., 2017) enabled the material to be highly mobile southeastward around the eastern Himalaya Syntaxis. Fluvial incision and rearrangement in response to regional uplift are probably among the few useful avenues to date and quantify these geodynamic models, which are important to understand their roles in crustal deformation (Clark et al., 2004; Yang et al., 2020; Zhao et al., 2021).

In the southeast Tibet, fluvial/lacustrine sediments, hundreds of meters thick, are widely distributed along the trunk of the upper course of the Yangtze River and its tributaries: the Yalung River, Dadu River, and Anning River, described as the Xigeda layer in Chinese literature. The occurrence of these sediments suggests large-scale blocking of paleo-rivers associated with locally tectonic activities (Clark et al., 2004; Clift et al., 2006; Deng et al., 2020; Zhao et al., 2021). However, owing to their depositional discontinuity and lack of fossils and isotopic dating, how and when these sediments were deposited are still up for debate. The nature of the relationship between these sediments and late Cenozoic development of the regional river system in southeastern Tibet remains an open question.

The mechanisms that drove deposition of the Xigeda Formation are greatly debated. As early as the 1950s, large-scale glacial development was considered as the main factor for the occurrence of these sediments during the Pliocene (Yuan, 1957). The hypothesis indicated that glaciations resulted in the valley geomorphology that is present along the modern Anning River; thus, the broad valley accommodated deposition of the Xigeda Formation. Thereafter, based on sedimentary and tectonogeomorphic characteristics, previous studies inferred that the late Cenozoic planation was disintegrated by neotectonics, resulting in linear distribution of the Xigeda paleo-lakes (Chen and Zhao,
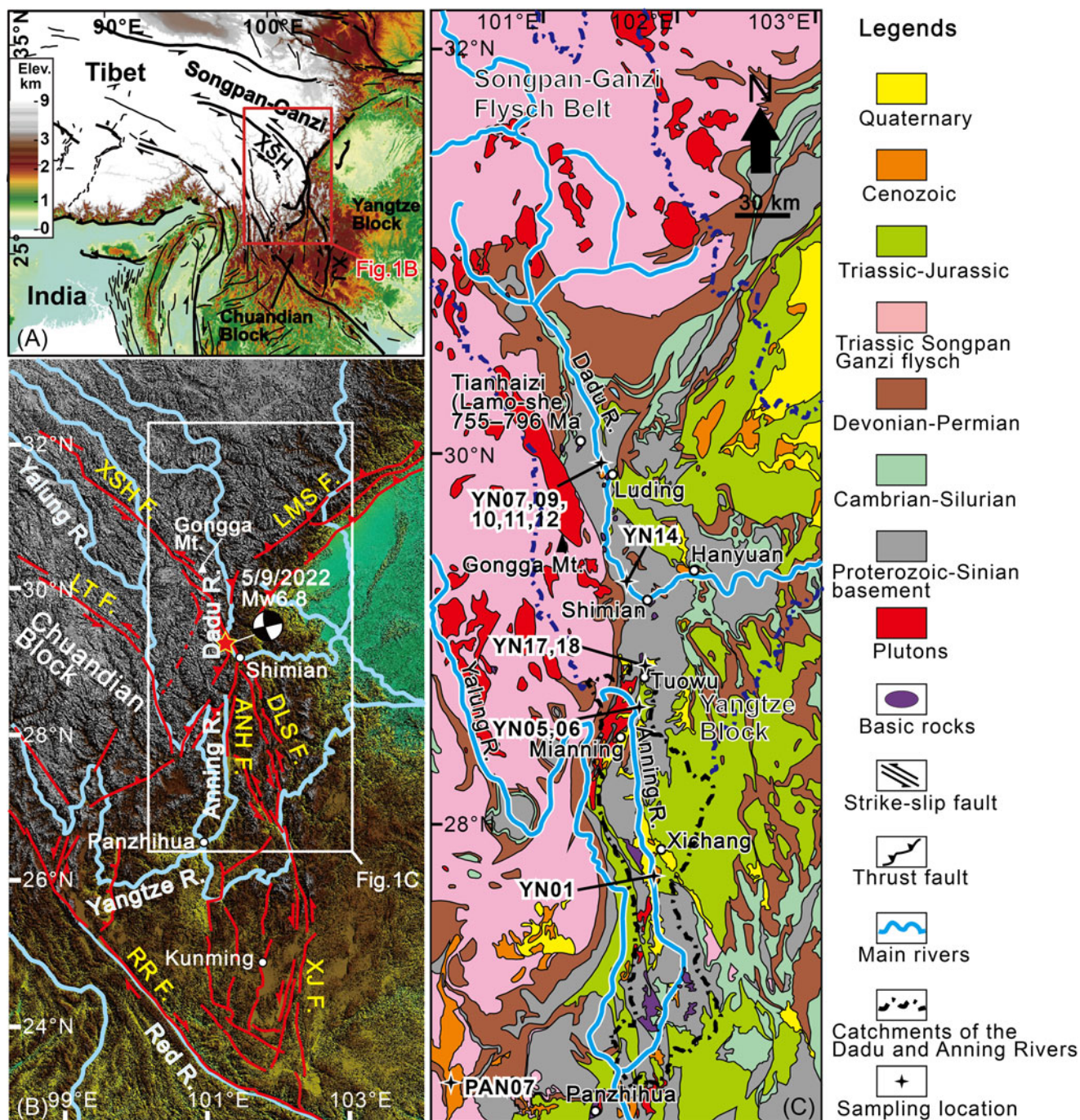
Figure 1. Tectonic and geological setting of southeast Tibet. (**A**) Topography and major faults of the central and eastern Tibetan Plateau. (**B**) Topography, major rivers, and active faults in southeastern Tibet. The 5/9/2022 Mw 6.8 Luding earthquake is based on China Earthquake Networks Center. XSH F. = Xianshuihe fault; DLS F. = Daliangshan fault; ANH F. = Anninghe fault; XJ F. = Xiaojiang fault; LMS F. = Longmenshan fault; LT F. = Litang fault; RR F. = Red River fault. (**C**) Geological map showing the main catchments of the Dadu and Anning rivers, and the sampling locations of this study. The Dadu River originates from the Bayan Har Mountains, drains southward to Shimian on the low-relief southeastern Tibetan Plateau. At Shimian the river abruptly makes a 90° turn, flowing eastward into the Sichuan Basin. South of Shimian, a wide valley appears in the headwaters region of the Anning River.

1989; Zhang, 1994). Wang and Burchfiel (2000) further suggested that those Xigeda paleo-lakes, which primarily developed at the bending of large strike-slip faults, are generally related to strike-slip extension. In contrast, Kong et al. (2009), Xu (2011), and Z.J. Zhang et al. (2017) provided direct evidence for the landslide-dammed genesis of the Xigeda Formation along the upper course of the paleo-Yangtze River, suggesting a large-scale river blocking.

Paleomagnetic dating of the Xigeda Formation initially suggested a depositional age ranging between 3.29–1.78 Ma (Qian et al., 1984). This method subsequently was widely applied in the dating of the Xigeda sediments in different locations, with results ranging from 4.3 Ma to 2.6 Ma (Luo and Liu, 1998; Jiang et al., 1999; Wang et al., 2006; Yao et al., 2007). However, determination of an absolute age was difficult,

considering that most sections only record normal-polarity paleomagnetic signals.

Given the large differences within the same strata, electron spin resonance (ESR) dating of the Xigeda Formation has been used only to test the paleomagnetic results (Yao et al., 2007; Wang et al., 2011). Kong et al. (2009) obtained 1.58–1.34 Ma for these fluvial/lacustrine sediments using cosmogenic nuclide burial dating, and thus, proposed a rearrangement of the middle Yangtze River during this period. Based on provenance and thermochronological studies, initial fluvial incision of the dammed lake and formation of the modern river system were inferred similarly before the early Pleistocene (Zhao et al., 2021). Clearly, constraint on the depositional age of the Xigeda sediments is a fundamental step toward understanding their origin and relationship to regional drainage changes in southeastern Tibet.

Although many studies have addressed the relationship between the deposition of these sediments and development of the fluvial system along the main trunk of the Yangtze River (Clift et al., 2006; Kong et al., 2009; Wei et al., 2016; Gourbet et al., 2017; Z.J. Zhang et al., 2017), little attention has been paid to the main tributaries. In particular, the Dadu River, originating from the Songpan-Ganzi terrane separated from the upstream part of the Yellow River by the Bayan Har Mountains, first flows south along its upper course, then abruptly east, forming a ~90° bend at Shimian County (Fig. 1B). From here, it is separated from the headwaters of the ~N-S Anning River by a low, wide pass (Yang et al., 2020). Therefore, the occurrence of river capture near Shimian from the paleo-Dadu-Anning River has been suggested (Clark et al., 2004; Deng et al., 2020; Yang et al., 2020; Zhao et al., 2021). Available low-temperature thermochronology data have suggested that the middle and upper courses of the Yangtze River widely experienced a rapid incision prior to or coeval with the middle–late Miocene, which corresponds to plateau uplift (Clark et al., 2004, 2005; Ouimet et al., 2010; Wang et al., 2012; Zhang et al., 2016; Cao et al., 2019). In contrast, a study on the Gongga batholith revealed a rapid exhumation since ca. 4 Ma based on thermokinematic modeling, corresponding to activity of the Xianshuihe fault (Y.Z. Zhang et al., 2017). Combining thermochronometric data with topographic analysis, Yang et al. (2020) suggested that capture of the paleo-Dadu–Anning River caused possible enhanced cooling since ca. 2 Ma. Such a rapid cooling since the early Quaternary also was discovered along the adjacent Anning River and Three River region (Liu-Zeng et al., 2018; Replumaz et al., 2020; Wang et al., 2021; Shen et al., 2022), which resulted from locally focused uplift and faulting activities.

In this study, we utilize cosmogenic nuclide burial dating to constrain the time of rearrangement of the Dadu River by dating the Xigeda fluvial/lacustrine sediments that occur along the modern Dadu and Anning River valleys. Via the analyses of detrital zircon U-Pb age distributions, the provenance and origin of the Xigeda Formation is further discussed. Synthesizing this information, we hope to explore their implications in regional neotectonic movement and geodynamic models in southeastern Tibet.

GEOLOGICAL SETTING AND SAMPLING

The southeastern margin of Tibet is characterized by a uniquely continuous and low gradient compared with the other margins of the Tibetan Plateau (Figs. 1A, B). Within this area, both the Anning and Dadu rivers are the major tributaries of the

Yangtze River. Their drainage areas mainly consist of two geological units (Fig. 1C). The eastern unit belongs to the Yangtze Block, and its basement is constituted by Neoproterozoic flysch, sodic volcanic rocks, and carbonates (Li et al., 2003). The sedimentary cover is thin with weak magmatism and varies from clastic rocks, carbonates, basic volcanic rocks, and coal-bearing layers of the marine-terrigenous environment of the Sinian–Late Triassic to continental sedimentation dominated by the coal-bearing molasse and red clastic rocks of the Late Triassic–Cenozoic. The Songpan-Ganzi flysch belt constitutes the western unit and was developed from a large foreland basin during the Triassic orogeny (Xu, 1992), which was accompanied by extensive magmatism (Roger et al., 2004; de Sigoyer et al., 2014). Flysch sediments, as represented by deep-marine siliciclastic turbidites (Xu, 1992; Meng et al., 2005), constitute the main sedimentary cover.

Deformation in southeastern Tibet was characterized by frequent strike-slip faulting with different magnitudes during the late Cenozoic (Bai et al., 2018). Among them, the Xianshuihe-Anninghe-Xiaojiang fault constitutes the eastern boundary of the Chuandian Block that extends southeastward, corresponding to the convergence between Eurasia and India (Fig. 1B). The Xianshuihe fault constitutes the northern segment, and splits into two ~N-S left-lateral strike-slip branches near Shimian County: the Anninghe fault and the Daliangshan fault (Fig. 1B). The 5/9/2022 Mw 6.8 Luding earthquake occurred exactly within this transition zone. The Anning River flows southward along the ~N-S trending Anninghe fault.

The Xigeda fluvial/lacustrine sediments, which are widely found along the present-day Dadu and Anning river valleys (Fig. 1C), mainly consist of interbedded unconsolidated fine-grained sands, silts, and silty clays (Fig. 2A), with different elevations. Along the Dadu River, the fluvial/lacustrine sediments only occur upstream of Luding at 1800–2200 m asl, and downstream of Shimian at Hanyuan with elevations of 900–1100 m asl. Conglomerates lie unconformably beneath the lacustrine sediments in Luding (Fig. 2B). They are poorly sorted and sub-rounded with a maximum size of >1 m. Poorly sorted angular debris and conglomerates also occur as intercalated layers within the lower part of the lacustrine sediment section (Fig. 2C), suggesting dynamic conditions of lake formation during the early stage. Fluvial cobbles and sands are preserved overlying the lacustrine sediments as high terraces over the Dadu River (Fig. 2D).

Diamictites occur as high terraces on both sides of the Dadu River downstream of Luding (Fig. 3). The diamictites are largely composed of acidic igneous and metamorphic rocks. We found ultrabasic rocks within the diamictites at Daban, located at 1650–1800 m asl along national road 318. Opposite Daban, basic and ultrabasic rocks also appear in the diamictites at the village of Shangsong at similar elevations. According to local geological maps, ultrabasic rocks only lie on the west side of the Dadu River, opposite Luding town (Fig. 1C).

South of Shimian in Tuowu Village, fluvial sands crop out at the drainage divide of the Dadu and Anning rivers at ~2600 m asl along national road 108 (Fig. 4), ~1500 m higher than the current elevation of the Dadu River at Shimian. Away from the divide, the gradient of the headwater region of the Anning River decreases in steepness (from steep to more gentle gradients), suggesting regional uplift of the divide area (Yang et al., 2020).

South of Tuowu in Mianning County along the Anning River, fluvial sediments (~300 m thick) occur with a top elevation of 1972 m asl (Fig. 5A). This section shows a gray color in general and mainly consists of medium–fine sand layers with interbedded
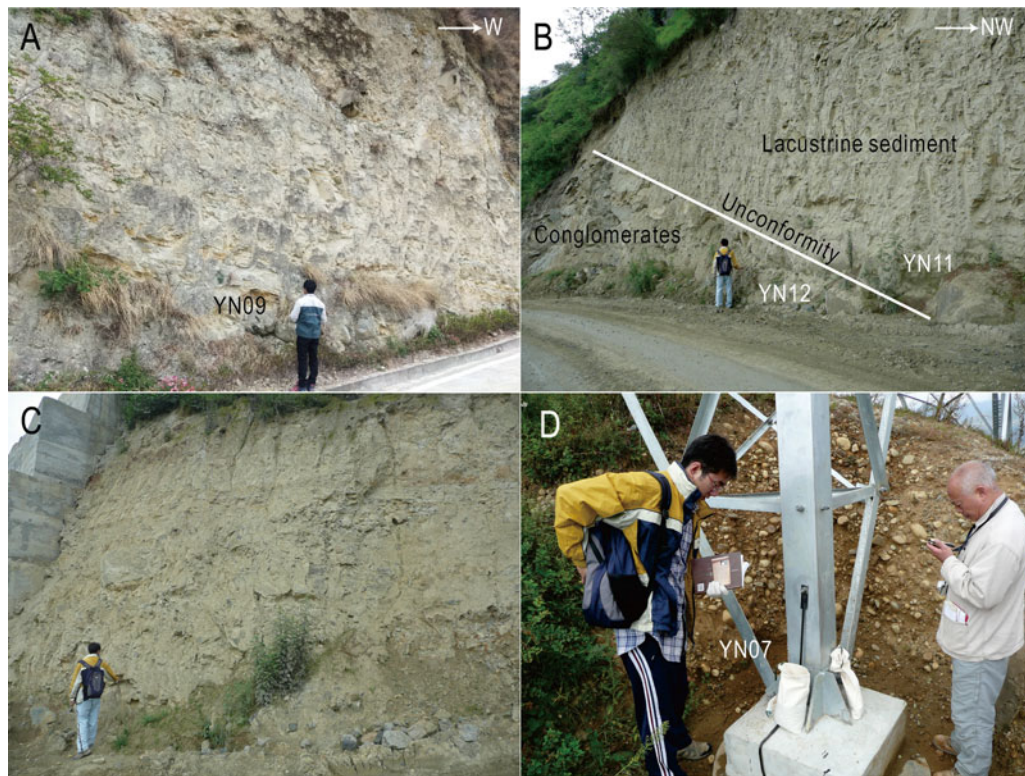
Figure 2. Sedimentary sequence at Haiziping, Luding. (**A**) Lacustrine sediments in the Haiziping section. (**B**) Unconformable contact between lacustrine sediments and the underlying poorly sorted and sub-rounded conglomerates. (**C**) Poorly sorted angular debris and conglomerates occur as intercalated layers within the lower part of the lacustrine sediments in the Haiziping section. (**D**) Fluvial cobbles and sands overlie the lacustrine sediments at Haiziping.

Figure 3. Relic dam related to lake formation around Luding. (**A**) The relic dam is preserved ~10 km downstream of Luding at the villages of Daban and Shangsong (based on picture derived from Google Earth). (**B**) Flat-topped surface of the relic dam on both sides of the Dadu River measures ~1800 m asl. (**C, D**) Ultrabasic rocks occur within the diamictites from upstream, west of Luding.
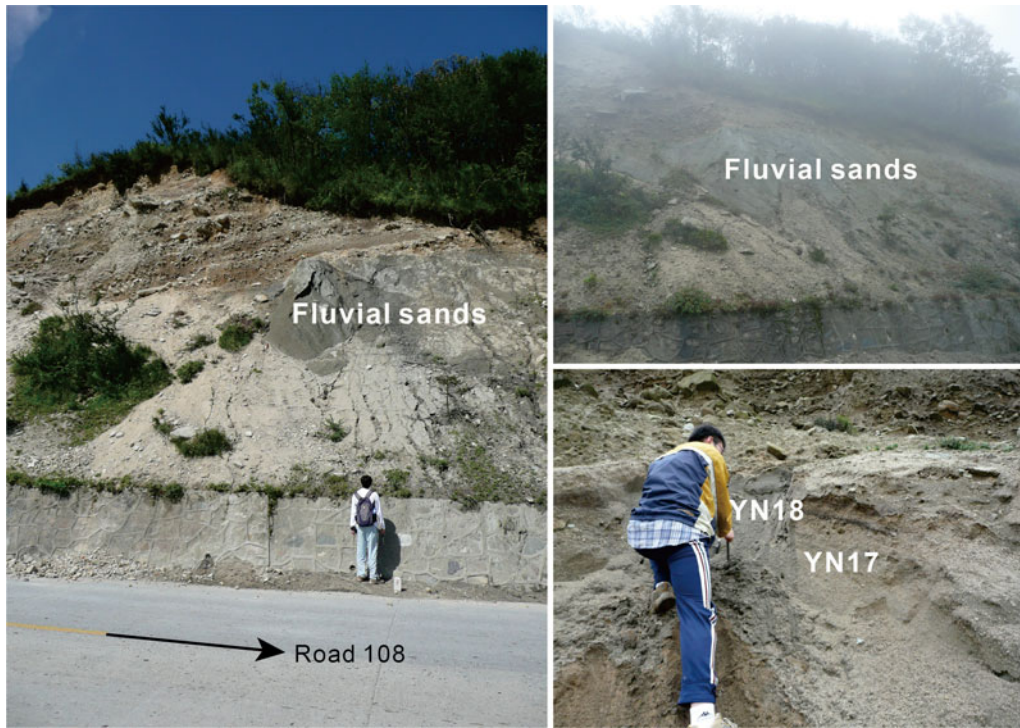
Figure 4. Fluvial sands collected at the drainage divide of the Dadu and Anning rivers in the village of Tuowu, south of Shimian. The fluvial sands outcrop at ~2600 m asl along national road 108.

Figure 5. Lacustrine sand samples collected at Zhoujiadagou, Mianning, and around Qionghai Lake, Xichang. (**A, B**) The Mianning section along an incised terrace is dark gray, which suggests reducing conditions. (**C, D**) Light-yellow silt and clay layers with development of horizontal laminations in the Xichang section, revealed by a construction slope.

silty clays (Fig. 5B). The sediments unconformably overlie the pre-Sinian metamorphic rocks.
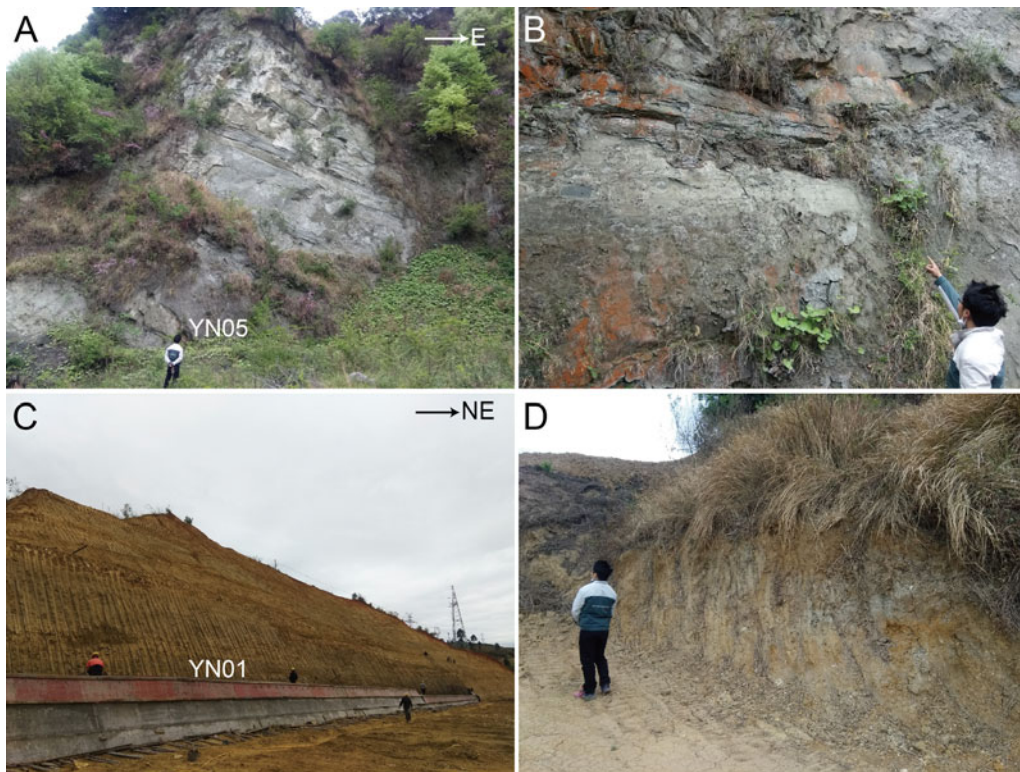
Southward around Qionghai Lake near Xichang, most sediments occur at elevations between 1600–1650 m asl, with thicknesses ranging from 140–200 m (Fig. 5C). The sediments are mainly composed of silt and clay layers with development of horizontal laminations (Fig. 5D). The Xigeda layers also occur continuously downstream of the Anning River between heights of 970–1500 m asl at Panzhihua (Kong et al., 2009).

Along the spiral road cut, we have collected five samples from the Haiziping section in Luding—from high to low: a fluvial sand sample overlying the lacustrine sediments, three lacustrine sediment samples, and a sample of lenticular sands embedded within the underlying conglomerates (Figs. 6, 7). We also collected a modern sand sample (YN14) from the lowest terrace of the Dadu River and two sand samples (YN17 and YN18) from the water divide that separates the Dadu and Anning rivers at the base of a road-cut (Fig. 4). Along the Anning River (Fig. 7), we collected two lacustrine sediment samples from the Zhoujiadagou section along an incised terrace in Mianning (YN05 and YN06), and one lacustrine sediment sample from the Xichang section at the base of a construction slope (YN01). Through statistical studies of detrital zircon U-Pb ages, together with cosmogenic nuclide burial dating of these samples, our goal is to decipher the mechanism of reorganization of the paleo-Dadu-Anning River and its relationship with the deformation mechanism of southeastern Tibet.

ANALYTICAL METHODS

Cosmogenic nuclide $^{26}Al/^{10}Be$ burial dating

Underlying methodology

Granger et al. (1997) first proposed an iterative solution for cosmogenic burial dating, and Granger and Smith (2000) elaborated this technique. The assumption behind the method is that, for a period of time, certain amounts of ^{10}Be and ^{26}Al are produced in quartz by cosmic rays near the ground surface (Lal and Arnold, 1985). The pre-burial $^{26}Al/^{10}Be$ ratio $N_{Al}(0)/N_{Be}(0)$ can be written as Equation (1), if the sample is collected from a steady-state eroding outcrop with a rate of ε:

$$N_{Al}(0)/N_{Be}(0) = P_{Al}(\lambda_{Be} + \varepsilon/\Lambda)/P_{Be}(\lambda_{Al} + \varepsilon/\Lambda) \qquad (1)$$

In Equation (1), P_{Al} and P_{Be} are the production rates of ^{26}Al and ^{10}Be, respectively; λ_{Al} and λ_{Be} are the decay constants, respectively. Λ refers to the attenuation length of neutrons.

After quartz is shielded from nuclide production and buried, the concentrations of ^{10}Be and ^{26}Al are then dominantly affected by decay. The concentrations of ^{10}Be and ^{26}Al after burial for time t become:

$$N_{Be}(t) = N_{Be}(0)e^{-\lambda_{Be} t} + N_{Be}(\text{depth})$$
$$\text{AND} \qquad (2)$$
$$N_{Al}(t) = N_{Al}(0)e^{-\lambda_{Al} t} + N_{Al}(\text{depth})$$

In equation (2), λ_{Be} and λ_{Al} are the decay constants of ^{10}Be and ^{26}Al, respectively; $N_{Be}(\text{depth})$ and $N_{Al}(\text{depth})$ are concentrations of ^{10}Be and ^{26}Al produced after burial, respectively. Because ^{26}Al has a shorter half-life than ^{10}Be, the ratio $N_{Al}(t)/N_{Be}(t)$ decreases exponentially over time. In this case, assuming that the sediments are buried rapidly enough and deeply enough to have no cosmogenic nuclide production, the measured $N_{Be}(t)/N_{Al}(t)$ can be expressed as:

$$N_{Al}(t)/N_{Be}(t) = N_{Al}(0)/N_{Be}(0)e^{(\lambda_{Be}-\lambda_{Al})t} \qquad (3)$$

In equation (3), $N_{Al}(0)$ and $N_{Be}(0)$ are pre-burial amounts of ^{26}Al and ^{10}Be, respectively, with a pre-burial erosion rate of ε. The concentrations of $N_{Al}(t)$ and $N_{Be}(t)$ are calculated from $^{26}Al/^{27}Al$ and $^{10}Be/^{9}Be$ ratios, respectively, determined by accelerator mass spectrometry (AMS). The convergence of burial time t, ε, and $N_{Al}(0)/N_{Be}(0)$ can be reached easily after a few iterations through Equations (1)–(3).

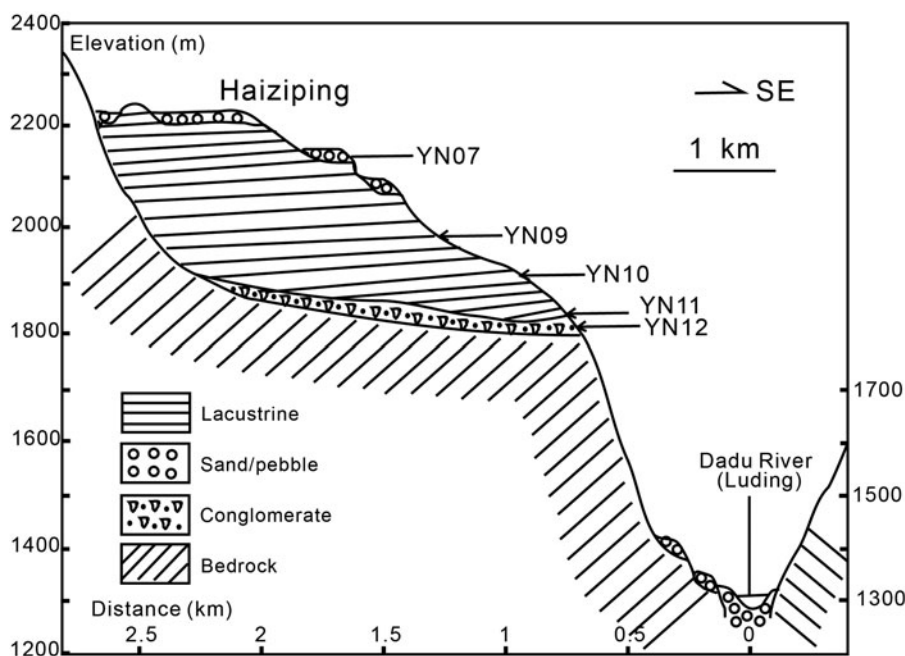**Figure 6.** Cross section of the Dadu River in Luding. Lacustrine sediments occur continuously from ~1800 m and to ~2200 m at Haiziping, which is 500–900 m higher than the current water level of the Dadu River in Luding. Fluvial sands and cobbles are preserved overlying the lacustrine sediments as high terraces above the Dadu River. We studied five samples (YN07, YN09–YN12) collected from the Haiziping section.
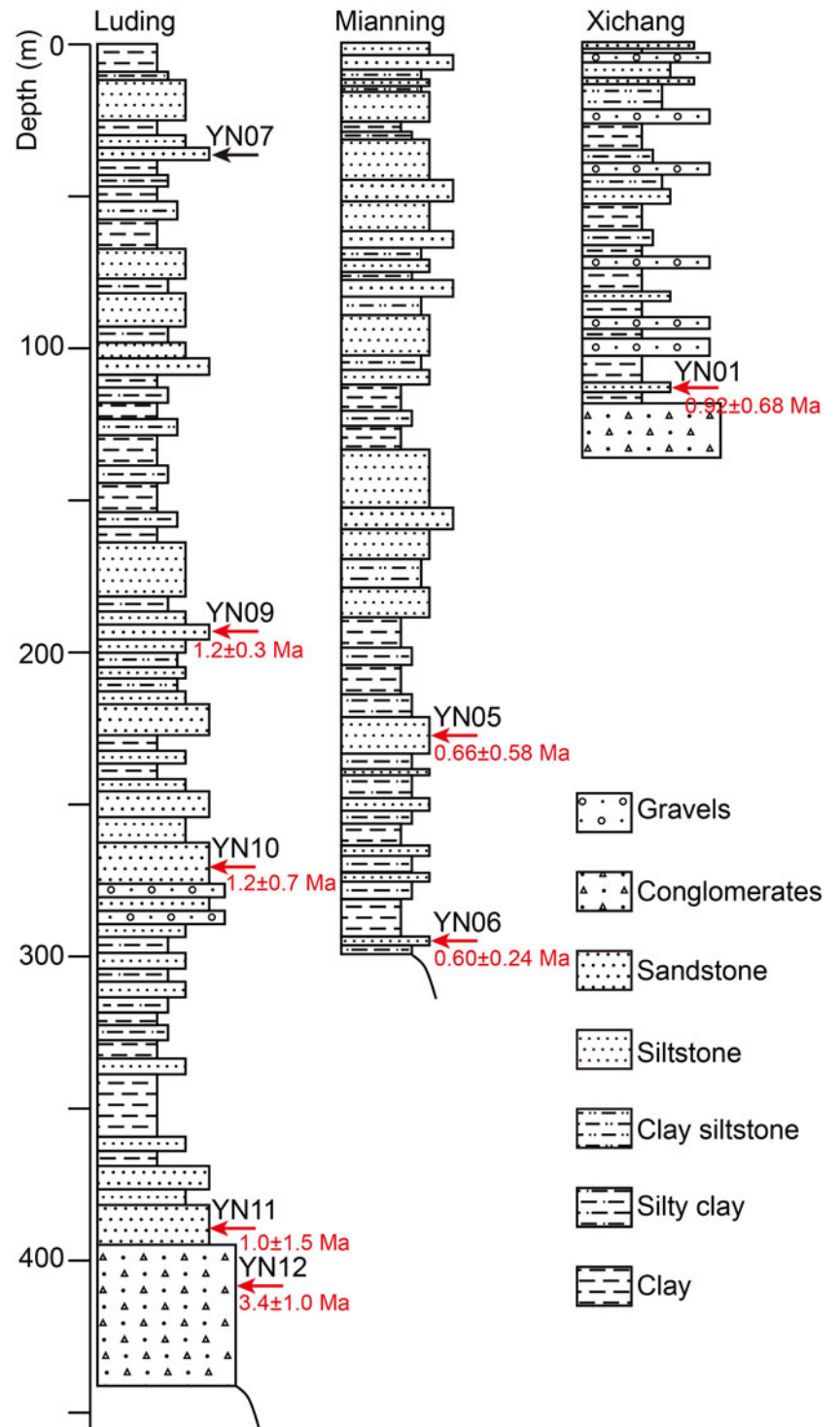
Figure 7. Xigeda fluvial/lacustrine sediment sections along the Dadu and Anning Rivers showing lithologies and samples collected during this study. This chart compiled paleomagnetic stratigraphies of the Luding, Mianning, and Xichang sections from Wang et al. (2006), Yao et al. (2007), and Zhang et al. (2013). Locations of samples collected for dating are marked with red arrows along with the age results; locations of samples collected for provenance analyses are marked with black arrows.

However, if quartz is buried at a limited depth and post-burial production of ^{10}Be and ^{26}Al needs to be taken into accounted, achieving an accurate burial age requires subtraction of the ^{10}Be and ^{26}Al produced since burial from $N_{Be}(t)$ and $N_{Al}(t)$ (Granger, 2014). $N_{Be}(\text{depth})$ and $N_{Al}(\text{depth})$ mainly consist of three components produced by nucleons, by fast muons, and by negative muons. Considering a landform with a constant post-burial erosion rate E (cm/yr), then those post-burial production of ^{10}Be and ^{26}Al can be modeled as a function of depth, as demonstrated by the following equations (Granger and Smith, 2000; Granger, 2014):

$$N_{Be}(\text{depth}) = P_{Be}[1 - e^{-(\lambda_{Be}+E/\Lambda)t}]e^{-z/L}/(\lambda_{Be} + E/\Lambda) +$$

$$B_1[1 - e^{-(\lambda_{Be}+E/\Lambda_1)t}]e^{-z/\Lambda_1}/(\lambda_{Be} + E/\Lambda_1) +$$

$$B_2[1 - e^{-(\lambda_{Be}+E/\Lambda_2)t}]e^{-z/\Lambda_2}/(\lambda_{Be} + E/\Lambda_2) +$$

$$B_3[1 - e^{-(\lambda_{Be}+E/\Lambda_3)t}]e^{-z/\Lambda_3}/(\lambda_{Be} + E/\Lambda_3)$$

AND

$$N_{Al}(depth) = P_{Al}[1 - e^{-(\lambda_{Al} + E/\Lambda)t}]e^{-z/\Lambda}/(\lambda_{Al} + E/\Lambda) +$$
$$A_1[1 - e^{-(\lambda_{Al} + E/\Lambda_1)t}]e^{-z/\Lambda_1}/(\lambda_{Al} + E/\Lambda_1)+$$
$$A_2[1 - e^{-(\lambda_{Al} + E/\Lambda_1)t}]e^{-z/\Lambda_2}/(\lambda_{Al} + E/\Lambda_2) +$$
$$A_3[1 - e^{-(\lambda_{Al} + E/\Lambda_3)t}]e^{-z/\Lambda_3}/(\lambda_{Al} + E/\Lambda_3) \qquad (4)$$

In equations (4), z is the burial depth of the sample. The adopted values for A_1, A_2, A_3, B_1, B_2, B_3, Λ_1, Λ_2, and Λ_3 in this study are summarized in Table 1. These parameters are described in detail in Granger (2014). Through assigning values for $N_{Be}(depth)$ and $N_{Al}(depth)$ into equation (2), only three unknowns (t, ε, and E) are remain. One of these unknowns—the post-burial erosion rate, E—has to be assumed in order to calculate the burial time t.

Additionally, if slow sedimentation with an accumulation rate of s (cm/yr) and post-burial production of cosmogenic nuclides also occur during the sedimentation process, cosmogenic nuclides are predominantly produced by neutron bombardment within a depth of 5 m. In this case, the accumulation of cosmogenic nuclides is basically the same as during the steady-state erosion process. If the accumulation duration (reaching a depth of 5 m) is short relative to the burial time t, then:

$$N_{Be}(depth, t) = P_{Be}e^{-\lambda_{Be}t}/(\lambda_{Be} + s/\Lambda)$$

AND

$$N_{Al}(depth, t) = P_{Al}e^{-\lambda_{Al}t}/(\lambda_{Al} + s/\Lambda) \qquad (5)$$

To calculate an appropriate burial age, one needs to obtain the sediment accumulation rate via an independent approach and further subtract $N_{Be}(depth, t)$ and $N_{Al}(depth, t)$ from $N_{Be}(t)$ and $N_{Al}(t)$, respectively.

Sample preparation
All physical and chemical preparations were performed at the cosmogenic nuclide laboratory at the Institute of Geology and Geophysics, Chinese Academy of Sciences in Beijing. Samples were first treated in 3N HCl for 6 hours on a hot plate to dissolve carbonate. Repeat-etching at 80°C with 1% HF:HNO$_3$ solution was adopted to remove meteoric ^{10}Be and to purify quartz. The purified quartz was then dissolved and spiked with a ~0.5 mg ^{9}Be carrier. Al concentrations were determined using the aliquots separated from the dissolved samples before HF volatilization and were measured by ICP-OES with a representative error of ±3% assigned to all Al concentrations between 17–185 ppm. ^{10}Be and ^{26}Al were progressively separated by anion exchange, acetyl acetone-CCl$_4$ using methods described in Kong et al. (2009). Al

Table 1. Adapted parameters for post-burial muonic production. These parameters, relating to equations (4) in the text, are taken from Granger and Muzikar (2001). The column numbers (1, 2, 3) are the subscripts of *L*, *A*, and *B*; ρ is the density of overburden sediments, which is taken as 2.5 g/cm^3 in this study.

	1	2	3
L	738/ρ	2688/ρ	4360/ρ
A	0.723	0.156	0.192
B	0.0846	0.0182	0.0230

cathodes were prepared by Al-Ag coprecipitation, and BeO was mixed with Nb. Accelerator mass spectrometry (AMS) measurements of ^{26}Al/^{27}Al and ^{10}Be/^{9}Be ratios were performed at the PRIME Lab, Purdue University. Ratios of ^{10}Be/^{9}Be are normalized to the ICN standard Be-01-5-2 with a ratio of 8.558×10^{-12}. All measured ^{10}Be/^{9}Be ratios were corrected for full chemistry procedural blanks prepared from purified solutions of beryl metal resulting in mean blank ^{10}Be/^{9}Be ratios of $(4.7 \pm 1.1) \times 10^{-15}$ (1σ). For ^{26}Al/^{27}Al ratios we used chemical blanks prepared from a pure Al solution to show ^{26}Al/^{27}Al ratios around the detection limit of $4×10^{-15}$ (1σ). Reported ^{10}Be and ^{26}Al concentrations include in quadrature a 2% reproducibility error of AMS standards. We used half-lives of 1.387 Ma and 0.705 Ma, and high-latitude, sea-level production rates of 4.6 atoms/g/yr and 31.1 atoms/g/yr are used for ^{10}Be and ^{26}Al, respectively, in the calculation.

Detrital zircon U-Pb age
Zircon grains were hand-picked after conventional heavy liquid and magnetic processing. Then, 200 grains were mounted in epoxy and polished to expose surfaces for optical and cathodoluminescence imaging. Zircon U-Pb dating was performed at the Institute of Geology and Geophysics, Chinese Academy of Sciences (IGGCAS), using an Agilent 7500a inductively coupled plasma mass spectrometer (ICP-MS) equipped with a Geolas 193 nm laser source. Detailed analytical and calculation procedures are described in Xie et al. (2008).

Within every ten zircon grains, standards 91500 and GJ-01 were measured twice for data correction and instrument status monitoring. NIST610 was used as an external calibration standard for rare element information. GLITTER 4.0 (Macquarie University) was used to calculate ^{207}Pb/^{206}Pb, ^{206}Pb/^{238}U, ^{207}Pb/^{235}U, and ^{208}Pb/^{232}Th ratios. Common Pb was corrected according to the method proposed by Andersen (2002).

RESULTS

Cosmogenic nuclide ^{26}Al/^{10}Be burial age

We dated nine lacustrine and fluvial sand samples taken from three sections and the drainage divide (Figs. 1C, 7): four samples from the Haiziping section in Luding (YN09, YN10, YN11, and YN12), two samples from the drainage divide in Tuowu village (YN17 and YN18), two samples from the Zhoujiadagou section in Mianning (YN05 and YN06), and one sample from the Xichang section (YN01). Sample information, ^{10}Be and ^{26}Al concentrations, and burial ages are given in Table 2. Compared with the isochron burial dating method, the simple burial dating method adopted in this study is based on more rigorous assumptions, such as: (1) simple burial history that samples are buried after only once exposure-burial process; (2) steady-state erosion environment; and (3) rapid burial (Granger and Smith, 2000). In particular, either the recycled material with early exposure history or slowly eroded material will result in a low initial ^{26}Al/^{10}Be ratio, which will cause overestimated burial ages if assuming a commonly used reference ratio of 6.75. However, our study areas and objectives still provide a nearly ideal configuration for the simple burial dating, because (1) the upper course of the Dadu River before it passes by Luding is characterized by a deeply incised gorge with a high average exhumation rate of ~0.33 mm/yr since ca. 9 Ma (Ouimet et al., 2010); (2) neither Neogene basins nor late Cenozoic sediments are widely developed along the upper

Table 2. Sample information and burial ages of the Xigeda samples associated with the Dadu and Anning Rivers. Density of sediments (ρ) is taken as 2.5 g/cm^3; penetration length of neutrons (Λ) is taken as 160 g/cm^2; half-lives of 1.387 Ma and 0.705 Ma, and high-latitude, sea-level production rates of 4.6 atoms/g/yr and 31.1 atoms/g/yr are used for ^{10}Be and ^{26}Al, respectively, in the calculations.

Sample	Latitude (N)	Longitude (E)	Elev. (m)	Depth (m)	^{10}Be/^{9}Be (×10^{-15})	^{26}Al/^{27}Al (×10^{-15})	^{10}Be (×10^4 atoms/g)	^{26}Al (×10^4 atoms/g)	^{26}Al/^{10}Be
YN09	29°54.966′	102°12.853′	2060	15	52.9 ± 2.8	83 ± 14	4.59 ± 0.23	18 ± 3	3.9 ± 0.7
YN10	29°54.284′	102°12.749′	1890	12	69.3 ± 2.6	28 ± 11	5.27 ± 0.21	21 ± 8	3.9 ± 1.5
YN11	29°54.176′	102°12.853′	1810	12	16.3 ± 1.0	8 ± 6	1.66 ± 0.10	7.8 ± 6.0	4.7 ± 3.6
YN12	29°54.200′	102°12.853′	1800	10	23.9 ± 1.2	14 ± 5	0.92 ± 0.05	2.1 ± 0.8	2.3 ± 0.9
YN17	28°53.994′	102°12.853′	2580	>10	32.6 ± 2.3	41 ± 10	1.33 ± 0.09	7.2 ± 1.7	5.4 ± 1.2
YN18	28°53.994′	102°12.853′	2580	>10	87.4 ± 3.4	27 ± 8	4.12 ± 0.16	23 ± 7	5.5 ± 1.6
YN01	27°45.580′	102°12.585′	1510	>15	162.1 ± 5.9	21 ± 6	14.46 ± 0.58	66 ± 20	4.6 ± 1.4
YN05	28°34.059′	102°12.633′	1730	18	46.1 ± 2.3	24 ± 7	3.32 ± 0.17	17 ± 5	5.1 ± 1.5
YN06	28°34.059′	102°12.634′	1810	18	61.9 ± 2.4	98 ± 13	4.50 ± 0.18	24 ± 3	5.3 ± 0.8

Sample	No post-burial production[a]			With post-burial production[b]			Slow sedimentation[c]		
	Burial age (Ma)	Pre-burial erosion rate (mm/kyr)	Pre-burial exposure age (ka)	Burial age (Ma)	Pre-burial erosion rate (mm/kyr)	Pre-burial exposure age (ka)	Burial age (Ma)	Pre-burial erosion rate (mm/kyr)	Pre-burial exposure age (ka)
YN09	1.1 ± 0.3	130 ± 7	4.7 ± 0.2	1.2 ± 0.3	130 ± 7	4.8 ± 0.2	1.2 ± 0.4	140 ± 8	4.4 ± 0.2
YN10	1.1 ± 0.7	99 ± 4	6.5 ± 0.3	1.2 ± 0.7	98 ± 4	6.5 ± 0.3	1.3 ± 0.9	100 ± 4	6.2 ± 0.3
YN11	0.95 ± 1.5	340 ± 21	1.9 ± 0.1	1.0 ± 1.5	330 ± 23	2.0 ± 0.1	1.1 ± 1.6	470 ± 37	1.4 ± 0.1
YN12	2.3 ± 0.7	300 ± 16	2.1 ± 0.1	3.4 ± 1.0	220 ± 13	3.0 ± 0.2	3.4 ± 1.5	250 ± 19	2.5 ± 0.2
YN17	0.45 ± 0.43	890 ± 60	0.7 ± 0.1	0.63 ± 0.58	870 ± 67	0.7 ± 0.1	0.80 ± 1.1	1600 ± 220	0.4 ± 0.1
YN18	0.43 ± 0.53	290 ± 11	2.2 ± 0.1	0.54 ± 0.59	290 ± 12	2.2 ± 0.1	0.67 ± 0.81	340 ± 16	1.9 ± 0.1
YN01	0.91 ± 0.66	32 ± 1	20.0 ± 0.8	0.91 ± 0.66	32 ± 1	20 ± 0.9	0.91 ± 0.67	32 ± 1	20 ± 0.8
YN05	0.62 ± 0.51	190 ± 10	3.4 ± 0.2	0.69 ± 0.66	190 ± 10	3.4 ± 0.2	0.73 ± 0.70	200 ± 12	3.1 ± 0.2
YN06	0.54 ± 0.21	160 ± 6	4.1 ± 0.2	0.60 ± 0.28	160 ± 6	4.2 ± 0.2	0.62 ± 0.30	170 ± 8	3.7 ± 0.2

[a]Minimum ages were obtained by assuming that the samples were completely shielded from cosmic rays after burial.
[b]Burial ages were obtained by assuming post-burial erosion rate of 300 m/Myr for samples. The higher erosion rate we assumed, the closer the burial ages to the minimum burial ages.
[c]Burial ages were obtained by assuming both post-burial erosion rate of 300 m/Myr and sedimentation rate of 180 m/Myr.

course (Fig. 1C); (3) the fluvial/lacustrine sediments are mainly located along the middle course of the Dadu River, from Luding to Shimian, and the Anning River valley along the Xianshuihe fault, indicating a clear affinity to the faulting activities; and (4) sediments with low initial ^{26}Al/^{10}Be ratios owing to a previous episode of burial generally show older burial age dates than obtained with geochronological constraints based on other methods, whereas our burial dating data are younger than the magnetostratigraphic dating results (Jiang et al., 1999; Wang et al., 2006; Yao et al., 2007) and are consistent with the local uplift period of the water divide since ca. 2 Ma (Yang et al., 2020). It is also worth noting that cosmogenic nuclide analyses in sediments from the present-day Dadu River and upper Yangtze River give ^{26}Al/^{10}Be ratios of 7.7 ± 4.8 and 6.2 ± 0.4 (2σ), respectively (McPhillips et al., 2016; Wittmann et al., 2020). The ^{26}Al/^{10}Be ratios of the Yangtze River sediments kept in the abandoned caves near the First Bend were measured at 6.3−7.1 (McPhillips et al., 2016), yielding burial ages between 18–9 Ma. As suggested by Kong et al. (2009), the paleo-Dadu drainage is one of the most important material sources for the Yangtze River near the First Bend before Pleistocene. Therefore, the pre-burial ^{26}Al/^{10}Be ratio adopted in this study that is equivalent to their production ratio of 6.75 is appropriate.

Minimum burial ages are simply calculated using equation (3). Because these samples were collected from sections with limited burial depths, ^{10}Be and ^{26}Al produced by muons and nucleons after burial need to be corrected (Granger, 2014). For buried samples that are within the range of muon production, the ^{10}Be and ^{26}Al concentrations are functions of the initial concentrations at the time of burial, the burial time, and the burial depth as a function of time. Thus, to calculate the burial time t, one unknown (e.g., E) has to be assumed. For longer timescales (>Ma), Yang et al. (2020) obtained an exhumation rate of 300−900 mm/kyr for the middle course of the Dadu River since ca. 2 Ma. Wang et al. (2021) reported a Quaternary change in erosion rates along the Anning River, with an average value of 300−400 mm/kyr. For shorter timescales, Chappel et al. (2006) estimated a ^{10}Be-based average catchment erosion rate of 300–500 mm/kyr for the Minjiang River, and Goddard et al. (2010) obtained similar erosion rates of 350–970 mm/kyr. Since ^{10}Be concentrations in modern sands taken from the Minjiang and the Dadu Rivers are similar (Chappel et al., 2006), and the hypsometric curves for the two catchments also are similar, the erosion rates for the two catchments should be similar. Additionally, based on the relationship between the mean basin slope and erosion rate, erosion rates of 330–1130 mm/kyr were directly estimated for the Dadu and Anning rivers (Ouimet et al., 2009). Assuming an erosion rate of 300 mm/kyr for locations where we collected the samples and taking into consideration post-burial production of ^{10}Be and ^{26}Al by negative and fast muons, we obtained burial ages for these samples, as shown in the Table 2. Given that these erosion rates are mainly based on basin-scale relief and the erosion rates increase toward the main channel below ∼2000 m (Ouimet et al., 2009; Yang et al., 2020), the 300 mm/kyr is a conservative estimate. The higher the erosion rate we assumed, the closer the burial ages were to the minimum burial ages (Fig. 8A; Supplementary Table S1). The simpler calculations have somewhat lower values than those with post-burial production, however the similarities (Fig. 8A) likely indicate that initial fast burial with certain pre-burial amounts of ^{10}Be and ^{26}Al is far more important than post-burial production and erosion in determining the inventory of cosmogenic nuclides.
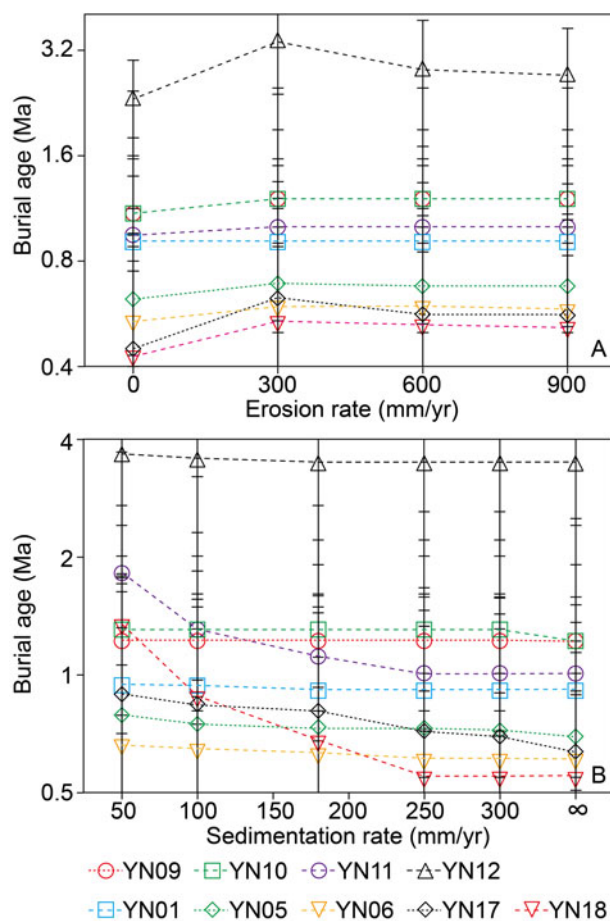

Figure 8. Calculation of burial ages of the Xigeda lacustrine sediments with various post-burial erosion rates and sedimentation rates. (**A**) Calculation of burial ages assuming post-burial erosion rates of 0, 300, 600, and 900 m/Myr. (**B**) Calculation of burial ages assuming a post-burial erosion rate of 300 mm/yr with sedimentation rates of very fast, 50, 100, 180, 250, 300 m/Myr.

Typically, if sediment accumulation rates are <30–100 mm/kyr, the post-burial production of ^{10}Be and ^{26}Al owing to slow sedimentation is a concern and should be taken into account (Zhang et al., 2014). We can estimate the accumulation rates of lacustrine sediments overlying the analyzed samples from the paleomagnetic results. A lacustrine sediment accumulation rate of ∼220 mm/kyr was suggested for the Luding Xigeda section (Wang et al., 2006), and an accumulation rate of ∼180 mm/kyr was suggested for the Mianning section (Yao et al., 2007). These results indicate widely rapid accumulation conditions for the Xigeda fluvial/lacustrine sediments along the Dadu and Anning drainages. Thus, 180 mm/kyr is an appropriate estimate.

Using accumulation rates from 50–300 mm/kyr and equations (5), we recalculated all the burial ages. The results are almost identical to those only considering post-burial erosion rate (Table 2; Supplementary Table S2) once an accumulation rate >100 mm/kyr (Fig. 8B) is reached, indicating that the post-burial production of ^{10}Be and ^{26}Al during sedimentation is negligible. However, for samples YN17 and YN18, which were collected from the divide, it might not be correct to assume rapid sedimentation rates since they are fluvial deposits (Fig. 4). We recalculate the burial ages for these samples, and the results increased to 0.89−1.31 Ma (Supplementary Table S2), if assuming a sedimentation rate of 50 mm/kyr (Fig. 8B). Therefore, the data in Table 2 are minimum values.

Most samples for cosmogenic nuclide burial dating were collected near the bottom of the fluvial/lacustrine sections (Fig. 7), thus, the burial ages most likely represent the initial formation of the Xigeda paleo-lake. Additionally, for the Luding section, three lacustrine sediments are taken from different elevations: YN09 at 2060 m, YN10 at 1890 m, and YN11 at 1810 m (Figs. 6, 7). The burial ages of the three lacustrine samples coincide within 1σ errors, indicating rapid accumulation; the two samples having smaller errors, YN09 and YN10, show identical ages, 1.2 ± 0.3 Ma and 1.2 ± 0.7 Ma, respectively. Taken as a weighted mean, the lake related to the lacustrine sediments in Luding formed 1.2 ± 0.3 Ma ago. The lenticular sand sample YN12 has a minimum burial age of 2.3 ± 0.7 Ma, and a burial age of 3.4 ± 1.0 Ma. Thus, the conglomerates underlying the lacustrine sediments were deposited on bedrock as an alluvial phase in the early Quaternary or Late Pliocene.

The limited variances of the $^{26}Al/^{10}Be$ ratios resulted in large errors of the burial ages for the Anning River drainage. However, all three samples were collected from burial sections with relatively deep depth to reduce the post-burial production effects; and both samples YN05 and YN06 were collected from different elevations in the Mianning section (Fig. 7)—YN05 at 1730 m and YN06 at 1810 m have $^{26}Al/^{10}Be$ ratios consistent with each other. Thus, the burial ages of these samples should be still usable. The burial age of the Mianning section is constrained at ca. 0.6 Ma ago and that of the Xichang section is constrained at ca. 0.9 Ma ago.

Detrital zircon U-Pb age distribution

Grains with Th/U ratios >1.0 represent an igneous origin, and $^{207}Pb/^{235}U$ versus $^{206}Pb/^{238}U$ ages concordant within 10% were used to infer the provenance information (Supplementary Table S3). For concordant analyses, $^{207}Pb/^{206}Pb$ ages were chosen for zircons older than 1 Ga (Compston et al., 1992), and for zircons younger than 1 Ga, $^{206}Pb/^{238}U$ ages were used in the statistical plots.

Seven samples were analyzed for their zircon U-Pb age distributions. Three were taken from the Haiziping section in Luding (Figs. 6, 7): the lacustrine sediment sample YN09, the fluvial sand sample overlying the lacustrine sediment (YN07), and the lenticular sand sample embedded within the conglomerates underlying the lacustrine sediment (YN12). One sample is from the modern sands of the Dadu River (Fig. 1C; YN14) and one sample is from the fluvial sands at the drainage divide (Fig. 4; YN18). Two samples were taken from along the Anning River drainage in lacustrine sediments at the Mianning section (Figs. 1C, 7; YN06) and the Xichang section (YN01), respectively. As shown in Figure 9, YN01, YN07, YN09, and YN18 display similar histogram patterns, showing main age populations between 160–320 Ma peaking at ca. 250 Ma, 720–880 Ma peaking at ca. 800 Ma, 1760–1920 Ma peaking at ca. 1800 Ma, and 2240–2560 Ma peaking at ca. 2500 Ma. The modern sand sample (YN14) and the young lacustrine sample (YN06) taken from the Mianning section display similar spectra with ages mainly peaking at 250 Ma and 800 Ma. Compared with the modern sand sample (YN14), the lenticular sand sample (YN12) shows a distinct spectrum with a single peak at 750 Ma, suggesting that the conglomerates underlying the lacustrine sediments at Haiziping are totally derived from the local Mount Tianhaizi (Lamo-She, 6070 m asl, Figs. 1C, 3A), with U-Pb ages of 755−796 Ma (Zhou et al., 2002; Li et al., 2003).

DISCUSSION

Formations of separate dammed lakes along the paleo-Dadu-Anning drainage

Cosmogenic nuclide burial dating shows that the lacustrine sediments in Luding were deposited 1.2 ± 0.3 Ma ago and the lacustrine sediments in Mianning were deposited ca. 0.6 Ma ago. These ages differ significantly from 2.6–4.2 Ma reported by Jiang et al. (1999), Wang et al. (2006), and Yao et al. (2007) based on the magnetostratigraphic method. Two sets of paleomagnetic data were obtained for the Haiziping section, both show primarily normal polarity paleomagnetic signal with four layers of negative signal (Jiang et al., 1999; Wang et al., 2006). For the Zhoujiadagou section in Mianning, only three layers of negative signal have been discovered (Yao et al., 2007). However, there are problems with these sets of data: (1) samples with negative signal are of very limited numbers; (2) negative signals only occur in coarse-grained layers; (3) negative signals appear at different positions, or depths, in the same section from the two sets of data; (4) no paleontological constraints were obtained to confine the time interval of the paleomagnetic data. Thus, the paleomagnetic age for the Haiziping and Zhoujiadagou sections needs to be seriously reconsidered.

Based on the distribution of the Xigeda fluvial/lacustrine sediments, Kong et al. (2009) suggested a large paleo-lake stretching 110 km from north to south and 160 km from east to west, formed as a result of a large landslide blocking the middle Yangtze River. Deng et al. (2020) argued for the existence of at least two large paleo-lakes at Panzhihua and Xichang. Although the detrital zircon U-Pb age distributions exhibit a similar material source for these fluvial/lacustrine sediments, the similar provenances are also consistent with the scenario that independent transient paleo-dammed lakes were filled with material carried by the integrated paleo-Dadu-Anning River.

In this study, three lacustrine samples for cosmogenic nuclide burial dating were collected from different elevations at the Luding section (Figs. 6, 7), and two samples were collected from the Mianning section with elevations at 1730 m and 1810 m. However, burial ages of the samples for each section overlap within 1σ errors. In addition, several fluvial/lacustrine samples of the Panzhihua section were dated previously with a large range of elevations (from 1058–1333 m; Kong et al., 2009). The burial ages also show a consistent result within errors. These results suggest that the Xigeda fluvial/lacustrine sediments formed from rapid accumulation. Some of these samples were collected near the bottoms of the sections (Fig. 7). Thus, the burial ages most likely represent the initial formation of the Xigeda paleo-lake, but not a continuous time-transgressive deposition. We propose that these fluvial/lacustrine sediments discontinuously occur at different regions deposited from separate transient paleo-dammed lakes, because: (1) the depositional ages differ significantly among these sediments—1.2 ± 0.3 Ma ago at Luding, ca. 0.6 Ma ago at Mianning, ca. 0.9 Ma ago at Xichang, and 1.6–1.3 Ma ago at Panzhihua (Kong et al., 2009); (2) the lacustrine sediments lie at different elevations—1800–2200 m near Luding, 1700–2000 m near Mianning, 1600–1650 m near Qionghai Lake, Xichang, and 970–1500 m continuously near Panzhihua; and (3) the redox states of the lacustrine sediments differ: the entire section of lacustrine sediments in Luding is khaki-colored visually (Fig. 2), both the Xichang and Panzhihua sections are light-yellow visually (Figs. 5C, D; Kong et al., 2009), whereas the Mianning section is dark-gray visually (Figs. 5A, B), suggesting reducing conditions. Therefore, considering that the Xigeda fluvial/lacustrine sediments were deposited during
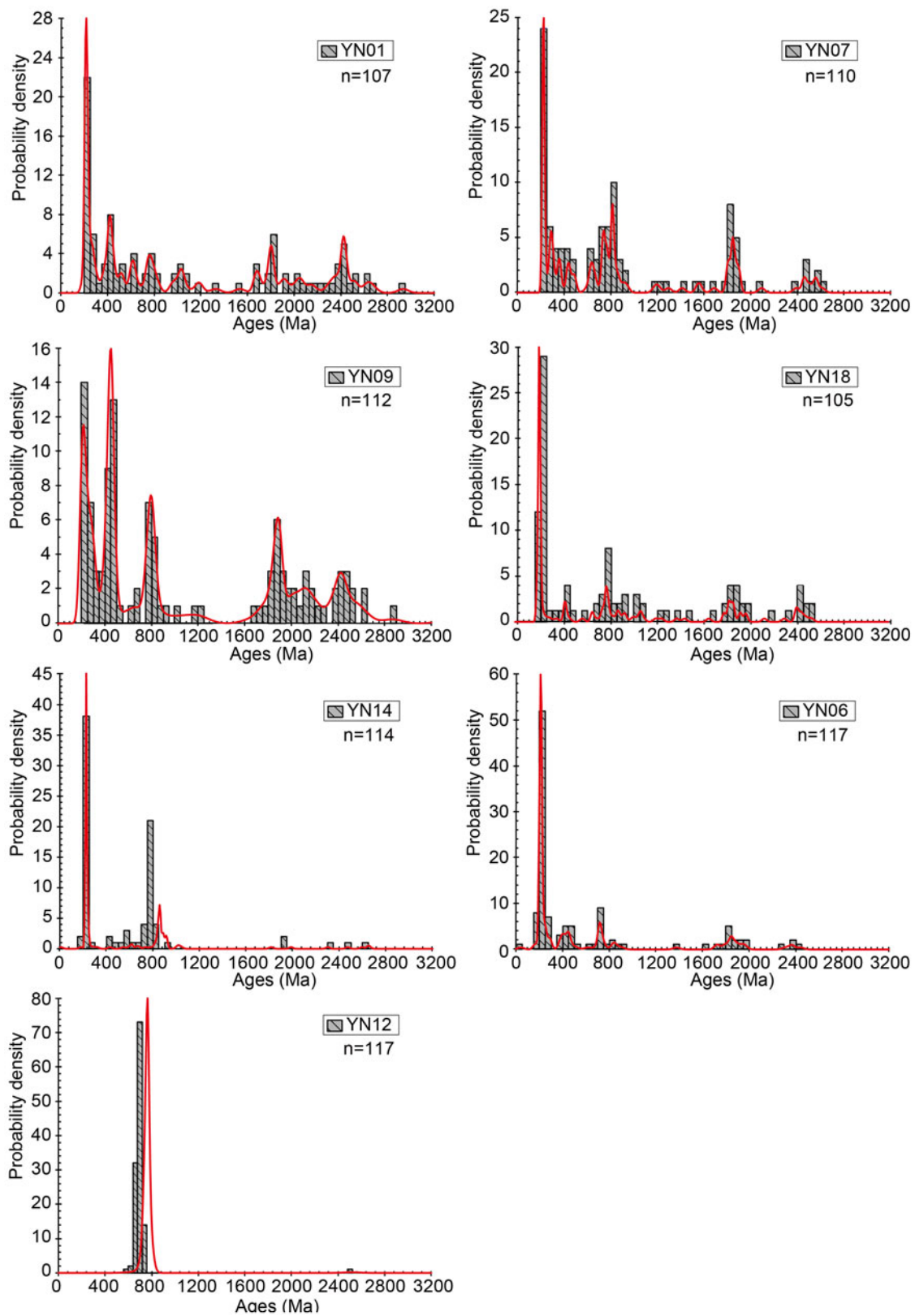
Figure 9. Distribution of detrital zircon U-Pb ages. Samples YN09, YN12, and YN07 were collected from the lacustrine layer, the lenticular sand within the conglomerates, and the fluvial sand overlying the lacustrine sediments at Haiziping, Luding, respectively; samples YN01 and YN06 were collected from the lacustrine sediments at Xichang and Mianning, respectively; sample YN14 is sand from the modern Dadu River; and sample YN18 is fluvial sand at the drainage divide in the village of Tuowu. Parameter n represents the number of analyzed concordant zircon grains used for the plots. The spectra of YN07, YN09, YN18, and YN01 are similar, with ages peaking at 250 Ma, 800 Ma, 1800 Ma, and 2500 Ma. The modern sand sample YN14 and sample YN06 lack paleo-Proterozoic zircons. YN12 displays a single peak at ca. 750 Ma, suggesting derivation from Mount Tianhaizi.

different periods, at different localities, and under different redox conditions, they should have formed in individual dammed lakes and were neither an isochronous nor a continuous stratigraphic unit.

The thickest section of the Xigeda fluvial/lacustrine sediments is located at Haiziping near Luding, with a thickness of ~441 m, which thins out markedly toward the south, indicating a heterogeneous distribution. In addition, landslide masses underneath the Xigeda lacustrine sediments have been identified on both sides of the modern Dadu River south of Luding County (Fig. 3). Therefore, the Xigeda sediments around Luding most likely originated from a dammed lake associated with a paleo-landslide, with the dam located near the villages of Daban and Shangsong (Fig. 3). Similarly, river blocking caused by the landslide was also widely discovered along the upper course of the Yangtze River (Xu, 2011) and probably resulted in the formation of the Xigeda sediments around Panzhihua (Kong et al., 2009). In contrast, the deeply incised valley of the Anning River was considered to be a result of extensional deformation corresponding to post-orogenic collapse of the eastern margin of the Tibetan Plateau (Wang et al., 1998; He et al., 2008; Zhang et al., 2010). The extensional deformation, which caused the formation of the Anning graben, is defined by normal-fault boundaries. Therefore, the fluvial/lacustrine sediments at the Mianning and Xichang with a considerable number of interbedded layers associated with local landslides (Xu, 2011) were most likely related to paleo-dammed lakes associated with the background of regional depressions.

The elevation of the modern Dadu River in Luding is ~1300 m. From the burial age and the elevation difference we obtained an incision rate of ~420 mm/kyr for the Dadu River. This value is within the range of 250–500 mm/kyr obtained for the Dadu and Yalong rivers based on U-Th/He dates, apatite fission track (Clark et al., 2005; Yang et al., 2020), and ^{10}Be concentrations in modern sands (Quimet et al., 2009). This value also is comparable with the regional uplift rate of 330 ± 30 mm/kyr for the entire Dadu River drainage since 12–15 Ma based on the stream-power incision model (Ma et al., 2020). The similarity of incision rates for the Dadu and Yalong rivers lying on southeastern Tibet most likely suggests a unified river incision response to regional uplift.

Reorganization of the Dadu River

For comparison, the zircon U-Pb age distributions of the sands collected from the present-day Dadu and Anning rivers, and the fluvial/lacustrine sediments collected from the Luding, Mianning, Xichang, and Panzhihua sections representing the paleo-drainages, are shown in Figure 10. Previous studies of detrital zircons show that U-Pb ages of ca. 2500 Ma and ca. 1800 Ma are mainly derived from the Songpan-Ganzi flysch belt along the headwaters region of the modern Dadu River (Bruguier et al., 1997; Weislogel, 2008; Ding et al., 2013; He et al., 2014), which are considered to be related to the amalgamation and breakup of a pre-Rodinian supercontinent, respectively (Zhai and Liu, 2003). Abundant zircons derived from widespread emplacement of volcanic rocks during the late Permian–Triassic are also found in upper reaches of the Dadu River (Fig. 1C). Additionally, as one of the major juvenile crustal additions and reconstructions, Neoproterozoic pre-rifting magmatism is widely developed along the western margin of the Yangtze Block, which currently is along the Anning River and downstream of the Dadu River (Fig. 1C). The breakup of the Rodinia

supercontinent is regarded as the mechanism for the late stage (820–750 Ma) (Li et al., 2003), whereas the early stage (950–820 Ma) is related to an island arc setting. Along the modern Dadu and Anning drainages, the Neoproterozoic magmatic rocks are primarily composed of granulites, amphibolites, felsic gneisses, and gneiss granites with zircon ages of 721–864 Ma (Zhou et al., 2002). Therefore, the zircon age spectra of YN07, YN09, YN18, YN06, YN01, and PAN07 indicate provenances from the Songpan-Ganzi flysch belt, Neoproterozoic complexes, and late Permian and Triassic granite plutons. The similarity in zircon age spectra among YN07, YN09, and YN18 (Figs. 9, 10) indicates that the fluvial sand sample YN18, taken from the drainage divide in Tuowu (Fig. 4), is indeed a remnant of the paleo-Dadu River.

The presence of relic sands of the Dadu River in Tuowu suggests that the paleo-Dadu River originally flowed southward through Tuowu into the Anning River. Compared with the sands of the modern Anning River with a major Neoproterozoic peak (AN in Fig. 10), the zircon age spectra of the Xigeda sediments along the Anning River exhibit a prominent peak at ca. 250 Ma (YN06 and YN01 in Fig. 10). This is different from the source signal of the Anning drainage, but similar to the sands taken from the modern Dadu River and the sediments of the Luding section. The multidimensional scaling (MDS) plots for comparison of detrital zircon signatures between the Xigeda lacustrine/fluvial sediments and selected provenances (Fig. 11) also suggest that the detrital zircon signatures of the relic sands in Tuowu and along the Anning River are similar to those of the modern Dadu River, further confirming that the paleo-Dadu River once flowed south and integrated with the Anning River so that the two rivers once shared similar provenances. Currently, the sands collected at the divide lie at ~2600 m. Uplift of the terrain in Tuowu (Clark et al., 2004; Yang et al., 2020) forced the Dadu River to change its flow direction and flow eastward from Shimian. Compared with the lowest elevation of the lacustrine sediments in Luding, the terrain in Tuowu rose at least 800 m in the last 0.6 Ma. This gives an uplift rate of ≥1300 mm/kyr.

With depositional ages decreasing, both zircon age peaks of ca. 2500 Ma and ca. 1800 Ma weaken gradually (Fig. 10). The samples indicate migration away from the provenance position of the Songpan-Ganzi flysch belt and closer to that of the Triassic and late Permian volcanic rocks (Fig. 11). The modern sand sample (YN14) in particular has the only ages peaking at 250 Ma and 800 Ma (Figs. 9, 10), and the absence of Paleoproterozoic zircons thus suggests that the modern Dadu River lost its headwaters stretching to the north of the Songpan-Ganzi Basin. Sample YN14 was collected from the lowest terrace of the Dadu River, which is 10 m above the current water level. Such a sampling strategy should eliminate any possible bias in zircon selection due to hydropower station construction since 1966 along the Dadu River. Because the U-Pb age spectra of YN06 and YN18 still show the signals of 1800 Ma and 2500 Ma, the modern Dadu River must have lost its headwaters within the last 0.6 Ma. Therefore, reorganization of the Dadu drainage at Shimian and progressive loss of the headwaters of the Dadu River should have occurred almost simultaneously within the last 0.6 Ma.

Tectonic implications

Both the elevated drainage divide and over-steepened gradients of the headstream of the Anning River suggest that capture of the paleo-Dadu-Anning River near Shimian (Figs. 12A−D) resulted from regional surface uplift since ca. 2.0 Ma (Clark et al., 2004;
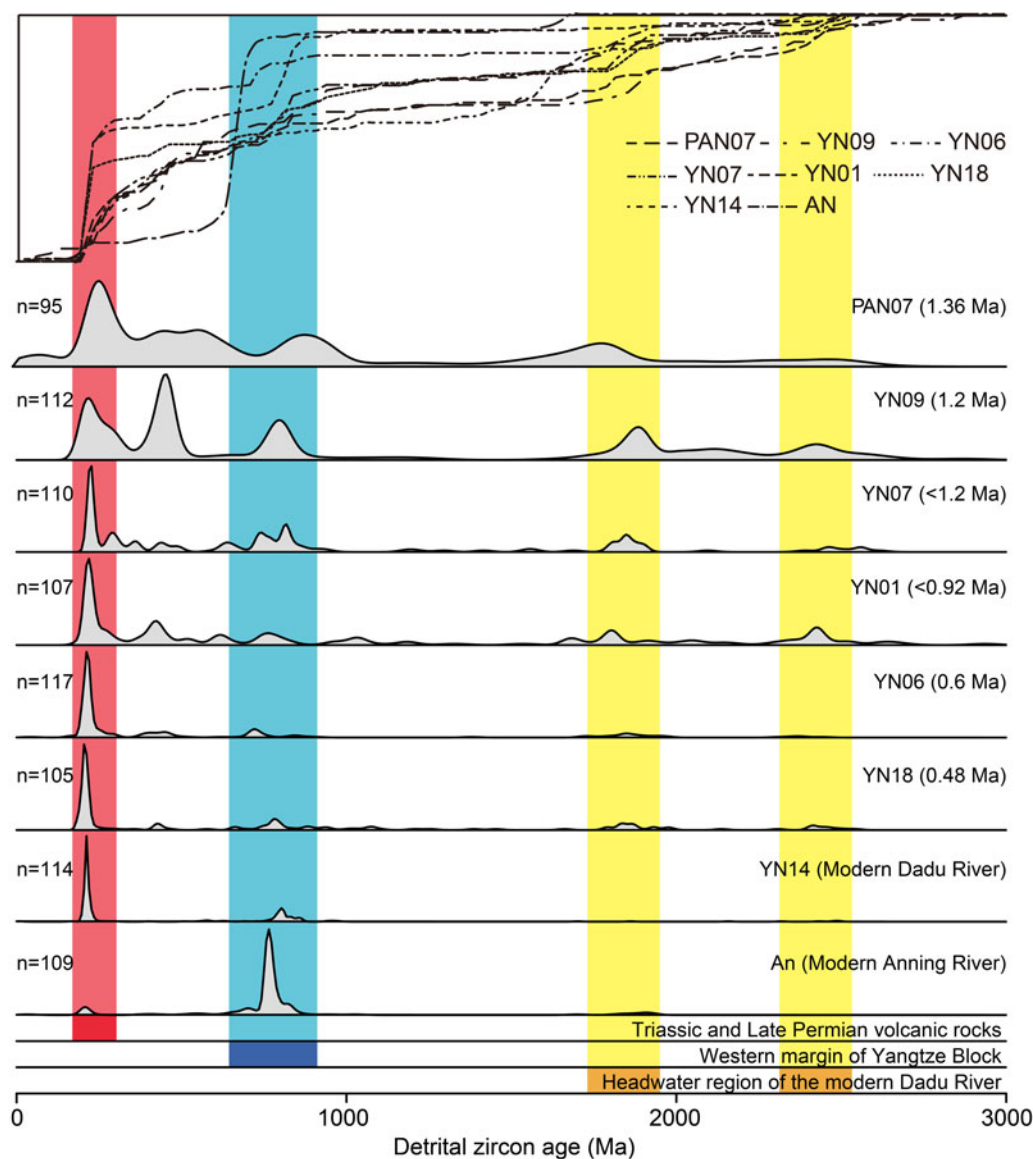
Figure 10. Diagram showing the distribution of detrital zircon ages from the Xigeda lacustrine sediments at different sections (PAN07, YN09, YN07, YN01, and YN06), the sands of the modern Dadu and Anning rivers (YN14 and AN), and the fluvial sands of the drainage divide between them (YN18). The sequence of lines in Figure 10 is based on the sedimentation age. Each curve contains all analyses from a single sample. Parameter n represents the number of analyzed concordant zircon grains used in each plot. The age distribution of the fluvial/lacustrine sediments in the Panzhihua section refers to Kong et al. (2009) and that of the modern Anning River refers to Yang et al. (2020). Vertical shaded bars show the main ages of zircons that would have been shed from various potential source regions. These age ranges have been compiled primarily from Bruguier et al. (1997), Zhou et al. (2002), Li et al. (2003), Weislogel (2008), Ding et al. (2013), He et al. (2014), and Xia et al. (2018).

Yang et al., 2020; Wang et al., 2021), which was completed within the last ca. 0.6 Ma, as determined by this study. Also, near Shimian, the Xianshuihe-Xiaojiang fault system turns from ∼SE trending into ∼N-S trending and splits into two major fault branches near the drainage divide—the Anninghe and Daliangshan faults (Fig. 12D). Both faults are characterized by a left-lateral slip with a dip-slip component (Wang et al., 1998), complexly sharing an ∼60 km left-lateral displacement to accommodate movement of the Xianshuihe-Xiaojiang fault system. Therefore, the drainage divide is located at the transition/bending zone along a large strike-slip fault, where it is apt to form a local surface uplift owing to the transpressional stress fields. With the regional surface uplift at the drainage divide associated with continuous strike-slip faulting, the southward flow of the

paleo-Dadu-Anning River was gradually blocked (Figs. 12A, C) and subsequently was captured and redirected toward the east near Shimian (Figs. 12B, D).

From the burial age and the elevation of the lacustrine sediments in Luding, we obtained an incision rate of 420 mm/kyr for the local area of the Dadu River. This value is similar to those previously obtained for the Dadu and Yalong rivers at ∼30°N (Clark et al., 2005; Ouimet et al., 2009; Ma et al., 2020; Yang et al., 2020; Wang et al., 2021). Based on vertical profiles of low-temperature thermochronology, an exhumation rate or incision rate of ∼100–600 mm/kyr was derived for the Three Rivers region (Liu-Zeng et al., 2018; Shen et al., 2022). For the low reaches of the Salween River, Gu et al. (2006) obtained incision rates of ∼600 mm/kyr based on [10]Be exposure dating of
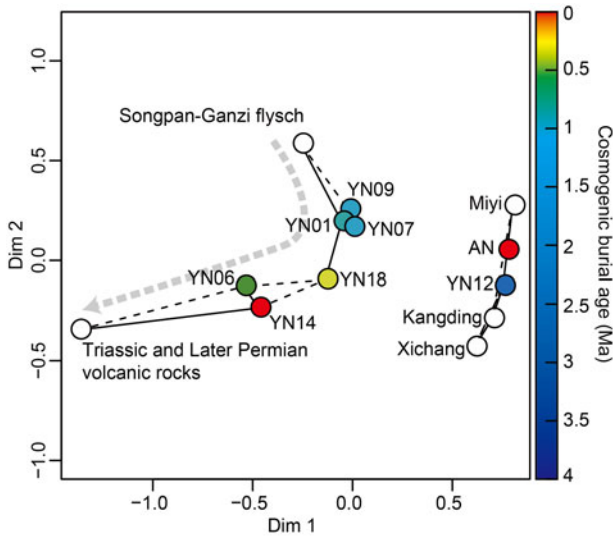
Figure 11. Two-dimensional multidimensional scaling plot of the fluvial/lacustrine sediments (color circles) along the Dadu and Anning rivers, and potential bedrock source units (hollow circles) (Bruguier et al., 1997; Zhou et al., 2002; Li et al., 2003; Weislogel, 2008; Ding et al., 2013; He et al., 2014; Xia et al., 2018). Samples are colored according to cosmogenic nuclide burial age. Dissimilarity is based on the K-S statistic D value. The gray arrow shows the general trend with time.

fluvial terraces. These results suggest that uplift of the middle segment of the Chuandian Block (26–28°N latitude) occurred at rates similar to regions where the Dadu and Yalong rivers flow at ~30°N. The consistent surface-uplift rates for southeastern Tibet reflect regional uplift associated with crustal thickening. If we assume that the river-incision rate equals the surface-uplift rate, we can estimate the rate of crustal thickening as well as net crustal material inflow based on Airy isostatic equilibrium. Calculation shows the crustal thickening in areas of 26–30°N at a rate of 2–3 km/Myr.

The Xianhuihe-Xiaojiang fault is the most active fault in southeastern Tibet, with the Chuandian Rhombic Block exhibiting an increase southward in left-lateral strike-slip rate. Calculations based on GPS results and neotectonic deformation show that the left-slip rate is 12–15 mm/yr for the Anninghe-Xiaojiang fault system (Y.Z. Wang et al., 2008), 10–16 mm/yr for the segment from Kanding to Shimian (Y.Z. Wang et al., 2008; Bai et al., 2021), ~10 mm/yr for the middle segment (Bai et al., 2018), and 6–8 mm/yr for the Ganzi and northern segments (Chevalier et al., 2017). The land surface at altitude at ~30°N, from Batang, Litang, to Luding, measures ~4000 m asl, and the underlying crustal thickness is ~57 km (C.Y. Wang et al., 2008; Dong et al., 2020). If the entire crust behaves coherently, the maximum net gain of crustal material from Kangding to the Xiaojiang fault, a distance of 400 km, will be (16–10) mm/yr × 57 km × 500 km = 0.17 km³/yr,
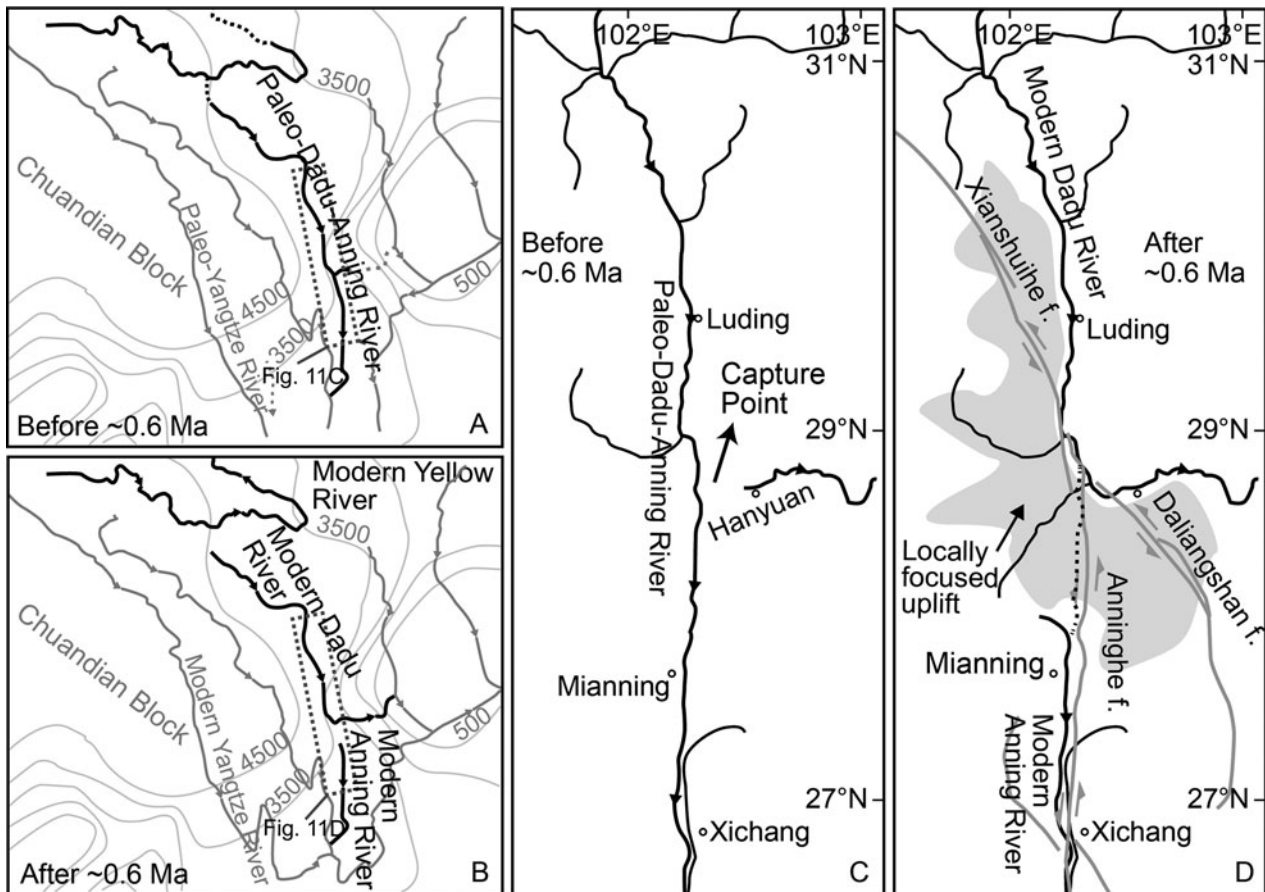

Figure 12. Summary of stream captures for the paleo-Dadu-Anning River. (**A**) Suggested recovered paleo-Dadu-Anning River pattern before reversal and capture, ca. 0.6 Ma ago. (**B**) Present-day river pattern after suggested capture events. (**C**) Recovered paleo-Dadu River once flowed directly south into the paleo-Anning River, constituting a ~N-S integrated paleo-Dadu-Anning River before ca. 0.6 Ma. (**D**) After the suggested capture due to locally focused uplift, the paleo-Anning River had its headwaters cut off, and the Dadu River was redirected toward the east.

considering a latitudinal width of 500 km. This value is much smaller than the material inflow calculated from the increase of crustal thickness, which is $(2$–$3)$ km/Myr $\times 400$ km $\times 500$ km $= 0.4$–0.6 km^3/yr. Such a mismatch suggests that the crust in southeast Tibet does not behave coherently so that the upper crust deformation is decoupled from the underlying weaker middle/lower crust in southeastern Tibet (Clark et al., 2005).

The tectonic uplift and rapid denudation since the late Miocene (5–12 Ma) were widely suggested by low-temperature thermochronology in eastern and southeastern Tibet (Clark et al., 2004; Wang et al., 2012; Zhang et al., 2016; Ma et al., 2020; Wang et al., 2021). Compared with the incision rate related to a longer history since the late Miocene, the millennial incision rates obtained by Ouimet et al. (2009) and this study and are consistent, implying that such a mechanical decoupling passing through the region of ~30°N likely occurred since 12–5 Ma.

Several models previously have been proposed to explain the geodynamics of the stream network reorganization that occurred in southeastern Tibet, including lateral extrusion of the Chuandian Block along large crustal-shearing faults (Leloup et al., 2001), gravitational spreading of the elevated crustal material (Copley, 2008), and dynamic channel flow within the lithosphere or asthenosphere (Clark and Royden, 2000; Shi et al., 2017). Based on the results in this study, these driving forces are not mutually exclusive and probably together resulted in a regional river network rearrangement associated with locally focused uplift. Particularly in southeastern Tibet, lateral rotation around the eastern Himalaya Syntaxis and extrusion of the Chuandian Block were largely decoupled from the kinematics of the middle/lower crust, causing formation of several large strike-slip fault systems, such as the Dali fault system, Xiaojiang fault system, and Xianshuihe fault system. As a result, these large-scale fault systems, which once transected the elevated planation into locally focused uplifts and depressions, consequently caused frequent paleo-drainage changes during the Pleistocene.

CONCLUSIONS

The geometry and evolution of fluvial systems are commonly found to be good proxies for crustal deformation processes and their related geodynamic mechanisms. Fluvial/lacustrine sediments with thicknesses of hundreds of meters are widely distributed along and above the present-day Dadu and Anning drainages in southeastern Tibet, providing sedimentary records of regional river network reorganization associated with late Cenozoic tectonic activities. Based on provenance analysis and cosmogenic nuclide burial dating, we reached three major conclusions.

First, based on cosmogenic nuclide burial dating, lacustrine sediments at the Luding, Mianning, and Xichang sections were deposited ca. 1.2 Ma ago, ca. 0.6 Ma ago, and ca. 0.9 Ma ago from north to south, respectively. The distinct ages and depositional environments of these sediments along the Dadu, Anning, and Yangtze rivers argue against the existence of a single contemporaneous lake in this area.

Second, detrital zircon U-Pb age distributions confirm that the fluvial sands at the drainage divide and the Xigeda sediments along the Anning River are the remnants of the paleo-Dadu River. Thus, the paleo-Dadu River originally flowed southward into the Anning River. Compared with the paleo-Dadu River, the modern sands of the Dadu River lack zircons with U-Pb ages of 1800 Ma and 2500 Ma, which are derived from north of

the Songpan-Ganzi Basin. Reorganization of the Dadu drainage and progressive loss of the headwaters of the Dadu River must have occurred within the last 0.6 Ma.

Third, over a million-year time scale, matching of material gain calculated from crustal thickening and slip-rates of surface faulting implies mechanical decoupling of the upper and middle/lower parts of the crust. The locally focused uplift driving rearrangement of the paleo-Dadu River also appears to be related to the compressional bending associated with Xianshuihe-Xiaojiang sinistral strike-slip faulting. Therefore, we propose that drainage reorganization in southeastern Tibet is related to a combination of several geodynamic processes, corresponding to the progressive convergence between the India and Eurasian plates.

REFERENCES

Andersen, T., 2002. Correction of common lead in U-Pb analyses that do not report ^{204}Pb. *Chemical Geology* **192**, 59–79.

Bai, M.K., Chevalier, M.L., Leloup, P.H., Li, H.B., Pan, J.W., Replumaz, A., Wang, S.G., *et al.* 2021. Spatial slip rate distribution along the SE Xianshuihe fault, eastern Tibet, and earthquake hazard assessment. *Tectonics* **40**, e2021TC006985. https://doi.org/10.1029/2021TC006985.

Bai, M.K., Chevalier, M.L., Pan, J.W., Replumaz, A., Leloup, P.H., Métois, M., Li, H.B., 2018. Southeastward increase of the late Quaternary slip-rate of the Xianshuihe fault, eastern Tibet. *Earth and Planetary Science Letters* **485**, 19–31.

Bruguier, O., Lancelot, J.R., Malavieille, J., 1997. U-Pb dating on single detrital zircon grains from the Triassic Songpan-Ganze flysch (Central China): provenance and tectonic correlations. *Earth and Planetary Science Letters* **152**, 217–231.

Cao, K., Wang, G., Leloup, P.H., Mahéo, G., Xu, Y., van der Beek, P.A., Replumaz, A., Zhang, K.X., 2019. Oligocene–early Miocene topographic relief generation of southeastern Tibet triggered by thrusting. *Tectonics* **38**, 374–391.

Chappel, J., Zheng, H.B., Fifield, K., 2006. Yangtze River sediments and erosion rates from source to sink traced with cosmogenic ^{10}Be: sediments from major rivers. *Paleogeography, Palaeoclimatology, Palaeoecology* **241**, 79–94.

Chen, F.B., Zhao, Y.T., 1989. *The Neotectonics in Panzhihua-Xichang Region of China*. Sichuan Science and Technology Publishing House, Chengdu. [in Chinese]

Chevalier, M.L., Leloup, P.H., Replumaz, A., Pan, J.W., Metois, M., Li, H.B., 2017. Temporally constant slip-rate along the Ganzi fault, NW Xianshuihe fault system, eastern Tibet. *Geological Society of America Bulletin* **130**, 396–410.

Clark, M.K., House, M.A., Royden, L.H., Whipple, K.X., Burchfiel, B.C., Zhang, X., Chen, L., 2005. Late Cenozoic uplift of southeastern Tibet. *Geology* **33**, 525–528.

Clark, M.K., Royden, L.H., 2000. Topographic ooze: building the eastern margin of Tibet by lower crustal flow. *Geology* **28**, 703–706.

Clark, M.K., Schoenbohm, L.M., Royden, L.H., Whipple, K.X., Burchfiel, B.C., Zhang, X., Tang, W., Wang, E., Chen, L., 2004. Surface uplift, tectonics, and erosion of eastern Tibet from large-scale drainage patterns. *Tectonics* **23**, TC1006. https://doi.org/10.1029/2002TC001402.

Clift, P.D., Carter. A., Campbell, I.H., Pringle, M.S., Lap, N.V., Allen, C.M., Hodges, K.V., Tan, M.T., 2006. Thermochronology of mineral grains in the Red and Mekong Rivers, Vietnam: Provenance and exhumation

implications for Southeast Asia. *Geochemistry, Geophysics, Geosystems* 7, Q10005. https://doi.org/10.1029/2006GC001336.

Compston, W., Williams, I.S., Kirschvink, J.L., Zhang, Z.C., Ma, G.G., 1992. Zircon U-Pb ages for the early Cambrian time-scale. *Journal of the Geological Society, London* 149, 171–184.

Copley, A., 2008. Kinematics and dynamics of the southeastern margin of the Tibetan Plateau. *Geophysical Journal International* 174, 1081–1100.

Deng, B., Chew, D., Mark, C., Liu, S.G., Cogné, N., Jiang, L., Sullivan, G.O., Li, Z.W., Li, J.X., 2020. Late Cenozoic drainage reorganization of the paleo-Yangtze river constrained by multi-proxy provenance analysis of the Paleo-lake Xigeda. *Geological Society of American Bulletin* 133, 199–211.

de Sigoyer, J., Vanderhaeghe, O., Duchêne, S., Billerot, A., 2014. Generation and emplacement of Triassic granitoids within the Songpan Ganze accretionary-orogenic wedge in a context of slab retreat accommodated by tear faulting, eastern Tibetan Plateau, China. *Journal of Asian Earth Sciences* 88, 192–216.

Ding, L., Yang, D., Cai, F.L., Pullen, A., Kapp, P., Gehrels, G.E., Zhang, L.Y., et al., 2013. Provenance analysis of the Mesozoic Hoh-Xil-Songpan-Ganzi turbidites in northern Tibet: Implications for the tectonic evolution of the eastern Paleo-Tethys Ocean. *Tectonics* 32, 34–48.

Dong, L., Shen, X.Z., Qian, Y.P., 2020. Study on velocity and density contrasts across the Moho in the southeastern margin of the Tibetan Plateau. *Chinese Journal of Geophysics* 63, 915–927. [in Chinese]

Godard, V., Lavé, J., Carcaillet, J., Cattin, R., Bourlès, D., Zhu, J., 2010. Spatial distribution of denudation in eastern Tibet and regressive erosion of plateau margin. *Tectonophysics* 491, 253–274.

Gourbet, L., Leloup, P.H., Paquette, J.L., Sorrel, P., Maheo, G., Wang, G.C., Xu, Y.D., et al. 2017. Reappraisal of the Jianchuan Cenozoic basin stratigraphy and its implications on the SE Tibetan Plateau evolution. *Tectonophysics* 700–701, 162–179.

Granger, D.E., 2014. 14.7—Cosmogenic nuclide burial dating in archaeology and paleoanthropology. In: Turekian, K., Holland, H. (Eds.), *Treatise on Geochemistry, second ed.* Elsevier Publishing, Amsterdam, pp. 81–97.

Granger, D.E., Kirchner, J.W., Finkel, R.C., 1997. Quaternary downcutting rate of the New River, Virginia, measured from differential decay of cosmogenic ^{26}Al and ^{10}Be in cave-deposited alluvium. *Geology* 25, 107–110.

Granger, D.E., Muzikar P.F., 2001. Dating sediment burial with in situ-produced cosmogenic nuclides: theory, techniques, and limitations. *Earth and Planetary Science Letters* 188, 269–281.

Granger, D.E., Smith, A.L., 2000. Dating buried sediments using radioactive decay and muogenic production of ^{26}Al and ^{10}Be. *Nuclear Instruments and Methods in Physics Research B: Beam Interactions with Materials and Atoms* 172, 822–826.

Gu, Z.Y., Xu, B., Lü, Y.W., Aldahan, A., Lal, D., 2006. ^{10}Be dating of terrace surfaces in Nujiang River valley. *Quaternary Sciences* 26, 293–294. [in Chinese]

He, H.L., Oguchi, T., 2008. Late Quaternary activity of the Zemuhe and Xiaojiang faults in southwest China from geomorphological mapping. *Geomorphology* 96, 62–85.

He, M.Y., Zheng, H.B., Bookhagen, B., Clift, P.D., 2014. Controls on erosion intensity in the Yangtze River basin tracked by U-Pb detrital zircon dating. *Earth-Science Reviews* 136, 121–140.

Jiang, F.C., Wu, X.H., Xiao, G.H., 1999. On the age of the Xigeda Formation in Luding, Sichuan, and its neotectonic significance. *Acta Geologica Sinica* 73, 6–13. [in Chinese]

Kong, P., Granger, D.E., Wu, F.Y., Caffee, M.W., Wang, Y.J., Zhao, X.T., Zheng, Y., 2009. Cosmogenic nuclide burial ages and provenance of the Xigeda paleo-lake: Implications for evolution of the Middle Yangtze River. *Earth and Planetary Science Letters* 278, 131–141.

Lal. D., Arnold, J.R., 1985. Tracing quartz through the environment. *Proceedings of the Indian Academy of Sciences—Earth and Planetary Sciences* 94, 1–5.

Leloup, P.H., Arnaud, N., Lacassin, R., Kienast, J.R., Harrison, T.M., Phan Trong, T.T., Replumaz, A., Tapponnier, P., 2001. New constraints on the structure, thermochronology, and timing of the Ailao Shan-Red River shear zone, SE Asia. *Journal of Geophysical Research, Solid Earth* 106, 6683–6732.

Leloup, P.H., Lacassin, R., Tapponnier, P., Schärer, U., Zhong, D.L., Liu, X.H., Zhang, L.S., Ji, S.C., 1995. The Ailao Shan-Red River shear zone

(Yunnan, China), Tertiary transform boundary of Indochina: *Tectonophysics* 251, 3–10, 13–84.

Liu-Zeng, J., Zhang, J.Y., McPhillips, D., Reiners, P., Wang, W., Pik, R., Zeng, L.S., et al., 2018. Multiple episodes of fast exhumation since Cretaceous in southeast Tibet, revealed by low-temperature thermochronology. *Earth and Planetary Science Letters* 490, 62–76.

Li, Z.X., Li, X.H., Kinny, P.D., Wang, J., Zhang, S., Zhou, H., 2003. Geochronology of Neoproterozoic syn-rift magmatism in the Yangtze Craton, South China and correlations with other continents: evidence for a mantle superplume that broke up Rodinia. *Precambrian Research* 122, 85–109.

Luo, Y.L., Liu, D.S., 1998. Study on depositional environment evolution and cyclic stratigraphy of Xigeda stratum. *Quaternary Sciences* 4, 373. [in Chinese]

Ma, Z.F., Zhang, H.P., Wang, Y.Z., Tao, Y.L., Li, X.M., 2020. Inversion of Dadu River bedrock channels for the late Cenozoic uplift history of the eastern Tibetan Plateau. *Geophysical Research Letters* 47, e2019GL086882. https://doi.org/10.1029/2019GL086882.

McPhillips, D., Hoke, G.D., Liu-Zeng, J., Bierman, P.R., Rood, D.H., Niedermann, S., 2016. Dating the incision of the Yangtze River gorge at the First Bend using three-nuclide burial ages. *Geophysical Research Letters* 43, 101–110.

Meng, Q.R., Wang, E., Hu, J.M., 2005. Mesozoic sedimentary evolution of the northwest Sichuan basin: Implication for continued clockwise rotation of the south China block. *Geological Society of America Bulletin* 117, 396–410.

Molnar, P., England, P., Martinod, J., 1993. Mantle dynamics, uplift of the Tibetan Plateau, and the Indian Monsoon. *Reviews of Geophysics* 31, 357–396.

Ouimet, W.B., Whipple, K.X., Granger, D.E., 2009. Beyond threshold hillslopes: channel adjustment to base-level fall in tectonically active mountain ranges. *Geology* 37, 579–582.

Ouimet, W.B., Whipple, K.X., Royden, L., Reiners, P., Hodges, K., Pringle, M., 2010. Regional incision of the eastern margin of the Tibetan Plateau. *Lithosphere* 2, 50–63.

Qian, F., Xu, S.J., Chen, F.B., Zhao, Y., 1984. Study on the paleomagnetism of the Xigeda Formation. *Mountain Research* 2, 275–282. [in Chinese]

Replumaz, A., San José M., Margirier, A., van der Beek, P., Gautheron, C., Leloup, P.H., Ou, X., et al. 2020. Tectonic control on rapid Late Miocene–Quaternary incision of the Mekong River knickzone, southeast Tibetan Plateau. *Tectonics* 39, e2019TC005782. https://doi.org/10.1029/2019TC005782.

Roger, F., Malavieille, J., Leloup, P.H., Xu, Z.Q., 2004. Timing of granite emplacement and cooling in the Songpan-Garzê Fold Belt (eastern Tibetan Plateau) with tectonic implications. *Journal of Asian Earth Sciences* 22, 465–481.

Shen, X.M., Braun, J., Yuan X.P., 2022. Southeastern margin of the Tibetan Plateau stopped expanding in the late Miocene. *Earth and Planetary Science Letters* 583, 117446. https://doi.org/10.1016/j.epsl.2022.117446.

Shi, X.H., Wang, Y., Sieh, K., Weldon, R., Feng, L.J., Chan, C.H., Liu-Zeng, J., 2017. Fault slip and GPS velocities across the Shan Plateau define a curved southwestward crustal motion around the eastern Himalayan syntaxis. *Journal of Geophysical Research, Solid Earth* 123, 2502–2518.

Wang, C.Y., Lou, H., Lü, Z.Y., Wu, J.P., Chang, L.J., Dai, S.G., You, H.C., Tang, F.T., Zhu, L.P., Silver, P., 2008. S-wave crustal and upper mantle's velocity structure in the eastern Tibetan Plateau—deep environment of lower crustal flow. *Science in China Series D: Earth Sciences* 51, 263–274.

Wang, E., Burchfiel, B.C., 2000. Late Cenozoic to Holocene deformation in southwestern Sichuan and adjacent Yunnan, China, and its role in formation of the southeastern part of the Tibetan Plateau. *Geological Society of America, Bulletin* 112, 413–423.

Wang, E., Burchfiel, B.C., Royden, L.H., Chen, L.Z., Chen, J.S., Li, W.X., Chen, Z.L., 1998. Late Cenozoic Xianshuihe/Xiaojiang and Red River fault systems of southwestern Sichuan and central Yunnan, China. *Special Paper, Geological Society of America Bulletin* 327, 1–108.

Wang, E., Kirby, E., Furlong, K.P., van Soest, M., Shi, X., Kamp, P.J.J., Hodges, K.V., 2012. Two-phase growth of high topography in eastern Tibet during the Cenozoic. *Nature Geoscience* 5, 640–645.

Wang, P., Li, J.P., Liu, C.R., Han, F., Gao, L., Wang, J.C., 2011. Quartz Ti-center in ESR dating of Xigeda formation in Sichuan and contrast

with magnetic stratigraphic profiles. *Nuclear Techniques* **34**, 111–115. [in Chinese]

Wang, S.B., Zhao, Z.Z., Qiao, Y.S., Jiang, F.C., 2006. Age and paleoenvironment of Xigeda Formation in Luding, Sichuan. *Quaternary Sciences* **26**, 257–264. [in Chinese]

Wang, Y.Z., Liu, C.R., Zheng, D.W., Zhang, H.P., Yu, J.X., Pang, J.Z., Li, C.P., Hao, Y.Q., 2021. Multistage exhumation in the catchment of the Anninghe River in the SE Tibetan Plateau: Insights from both detrital thermochronology and Topography analysis. *Geophysical Research Letters* **48**, e2021GL092587. https://doi.org/10.1029/2021GL092587.

Wang, Y.Z., Wang, E.N., Shen, Z.K., Wang, M., Gan, W.J., Qiao, X.J., Meng, G.J., *et al.*, 2008. GPS-constrained inversion of present-day slip rates along major faults of the Sichuan-Yunnan region, China. *Science in China Series D: Earth Sciences* **51**, 1267–1283.

Wei, H.H., Wang, E.C., Wu, G.L., Meng, K., 2016. No sedimentary records indicating southernly flow of the paleo-Upper Yangtze River from the First Bend in southeastern Tibet. *Gondwana Research* **32**, 93–104.

Weislogel, A.L., 2008. Tectonostratigraphic and geochronologic constraints on evolution of the northeast Paleotethys from the Songpan-Ganzi complex, central China. *Tectonophysics* **451**, 331–345.

Wittmann, H., Oelze, M., Gaillardet, J., Garzanti, E., von Blanckenburg, F., 2020. A global rate of denudation from cosmogenic nuclides in the Earth's largest rivers. *Earth-Science Reviews* **204**, 103147. https://doi.org/10.1016/j.earscirev.2020.103147.

Xia, Y., Xu, X.S., Niu, Y.L., Liu, L., 2018. Neoproterozoic amalgamation between Yangtze and Cathaysia blocks: the magmatism in various tectonic settings and continent-arc-continent collision. *Precambrian Research* **309**, 56–87.

Xie, L.W., Zhang, Y.B., Zhang, H.H., Sun, J.F., Wu, F.Y., 2008. In situ simultaneous determination of trace elements, U-Pb and Lu-Hf isotopes in zircon and baddeleyite. *Chinese Science Bulletin* **53**, 1565–1573.

Xu, Z.M., 2011. Deposits of Zhaizicun landslide-dammed lake along Jinsha River and its implication for the genesis of Xigeda Formation. *Geological Review* **57**, 675–686. [in Chinese]

Xu, Z.Q., 1992. *The Orogenic Process of Songpan-Ganzi Orogenic Belt, China.* Geological Publishing House, Beijing. [in Chinese]

Yang, R., Suhail, H.A., Gourbet, L., Willett, S.D., Fellin, M.G., Lin, X.B., Gong, J.F., *et al.*, 2020. Early Pleistocene drainage pattern changes in Eastern Tibet: constraints from provenance analysis, thermochronometry, and numerical modeling. *Earth and Planetary Science Letters* **531**, 115955. https://doi.org/10.1016/j.epsl.2019.115955.

Yao, H.T., Zhao, Z.Z., Qiao, Y.S., Li, C.Z., Wang, S.B., Wang, Y., Chen, Y.S., Jiang, F.C., 2007. Magneto stratigraphic dating of the Xigeda formation in Mianning, Sichuan and its significance. *Quaternary Sciences* **27**, 74–85. [in Chinese]

Yuan, F.L., 1957. A complementary study of evolution history of the Yangtze River. *Yangtze River* **2**, 3–11. [in Chinese]

Zhai, M.G., Liu, W., 2003. Palaeoproterozoic tectonic history of the North China craton: a review. *Precambrian Research* **122**, 183–199.

Zhang, H.P., Oskin, M.E., Liu-Zeng, J., Zhang, P.Z., Reiners, P.W., Xiao, P., 2016. Pulsed exhumation of interior eastern Tibet: implications for relief generation mechanisms and the origin of high-elevation planation surfaces. *Earth and Planetary Science Letters* **449**, 176–185.

Zhang, H.P., Zhang, P.Z., Champagnac, J., Molnar, P., Anderson, R.S., Kirby, E., Craddock, W.H., Liu, S.F., 2014. Pleistocene drainage reorganization driven by the isostatic response to deep incision into the northeastern Tibetan Plateau. *Geology* **42**, 303–306.

Zhang, J.X., 2013. The Nature of the Xigeda Ancestral Basin from Pliocene to Early Pleistocene in Panxi area, Sichuan Province. Master's Thesis, China University of Geosciences (Beijing), Beijing.

Zhang, Y.Q., Li, H.L., Li, J.H., 2010. Middle Pleistocene extension along the eastern margin of Xizang (Tibetan) Plateau and its neotectonic significance. *Geological Review* **56**, 781–791. [in Chinese]

Zhang, Y.Z., Replumaz, A., Leloup, P.H., Wang, G.C., Bernet, M., van der Beek, P., Paquette, J.L., Chevalier, M.L., 2017. Cooling history of the Gongga batholith: implications for the Xianshuihe Fault and Miocene kinematics of SE Tibet. *Earth and Planetary Science Letters* **465**, 1–15.

Zhang, Z.H., 1994. *Late Cenozoic Geology in Middle Segment of Sichuan-Yunnan South-North Tectonic Belt.* China Petroleum Press, Beijing. [in Chinese]

Zhang, Z.J., Daly, J.S., Li, C.A., Tyrrell, S., Sun, X.L., Yan, Y., 2017. Sedimentary provenance constraints on drainage evolution models for SE Tibet: evidence from detrital K-feldspar. *Geophysical Research Letters* **44**, 4064–4073.

Zhao, X.D., Zhang, H.P., Tao, Y.L., Wang, Y., Pang, J.Z., Ma, Y., Zhang, J.W., Ma, Z.F., Xiong, J.G., 2021. Pliocene to Early Pleistocene drainage reorganization in eastern Tibet inferred from detrital zircons. *Geophysical Research Letters* **48**, e2021GL094563. https://doi.org/10.1029/2021GL094563.

Zhou, M.F., Yan, D.P., Kennedy, A.K., Li, Y.Q., Ding, J., 2002. SHRIMP U-Pb zircon geochronological and geochemical evidence for Neoproterozoic arc-magmatism along the western margin of the Yangtze block, South China. *Earth and Planetary Science Letters* **196**, 51–67.